XUV view on ultrafast demagnetization

Boris Vodungbo

XUV view on ultrafast demagnetization

Habilitation à diriger des recherches soutenue par :

Boris Vodungbo

devant le jury composé de :

Pr. Martin Aeschlimann	Rapporteur
Pr. Davide Boschetto	Rapporteur
Dr. Catherine Gourdon	Présidente
Pr. Sophie Kazamias	Membre du jury
Dr. Thierry Ruchon	Rapporteur

11 Avril 2022

Contents

List of Figures

1. Introduction

The dynamic response of magnetic order to ultrafast optical excitation is a fascinating issue of modern magnetism. The temporal evolution of the magnetization evolving in the material pushed far out of equilibrium by the intense optical excitation can be resolved with femtosecond time resolution using optical probe techniques like magneto-optical Kerr effect (MOKE). Such experiments realized over the past two decades or so have provided us with detailed insight into the elementary interactions between spins, electrons, and lattice and their characteristic time scales as illustrated schematically in figure 1.1 (a) [3, 2, 4, 5, 6].

In the context of fundamental science, the phenomenon of ultrafast demagnetization of ferro- and ferrimagnetic materials, which was discovered by E. Beaurepaire, J.-Y. Bigot and their colleagues already in 1996 [2], remains until today at the focus of intense, world-wide research activities and controversial debates [7, 8, 9, 10, 11]. The open question underlying these debates concerns the mechanism of energy and angular momentum exchange with the spin system on a sub-picosecond time scale, which is necessary to dissipate the magnetic angular momentum associated with the ultrafast drop in magnetization (see figure 1.1 (b)). Whether the angular momentum is dissipated into the lattice via phonons or defects [1], whether it is carried away by hot electrons [12], or whether both mechanisms (or more) contribute is still investigated.

A fascinating discovery, which resulted from studies of ultrafast dynamics of magnetic systems, is the demonstration that the magnetization direction can be controlled with circularly polarized light pulses, without the presence of any applied magnetic field. This was first demonstrated in 2007 by the group of T. Rasing in Nijmegen, who employed single circularly polarized femtosecond laser pulses [13] to deterministically switch the magnetization of a thin ferrimagnetic GdFeCo alloy film. This remarkable phenomenon has been termed all-optical switching (AOS). We note that the AOS takes place on a timescale of a few tens of picoseconds [14], which is about two orders of magnitude faster than any other reported mechanism to manipulate the magnetization direction – with the notable exception of employing relativistic electron beams [15]. Thus, AOS is considered to have the potential of creating a disruptive technology development for a variety of applications. Moreover this process is highly energy efficient; an energy lower than 10 fJ is expected to be sufficient to switch a $20 \times 20\,\mathrm{nm}^2$ area of magnetic material [16]. This technological potential combined with the scientific interest in understanding the mechanism underlying this process has given rise to considerable research efforts.

Typically, experiments exploring ultrafast magnetization dynamics are performed as stroboscopic pump-probe measurements. The principle of pump-probe experiment is the following: (i) the system to be studied is pushed out of equilibrium by a stimulus, the pump; (ii) the state of the system is then measured, after a certain time delay, by the

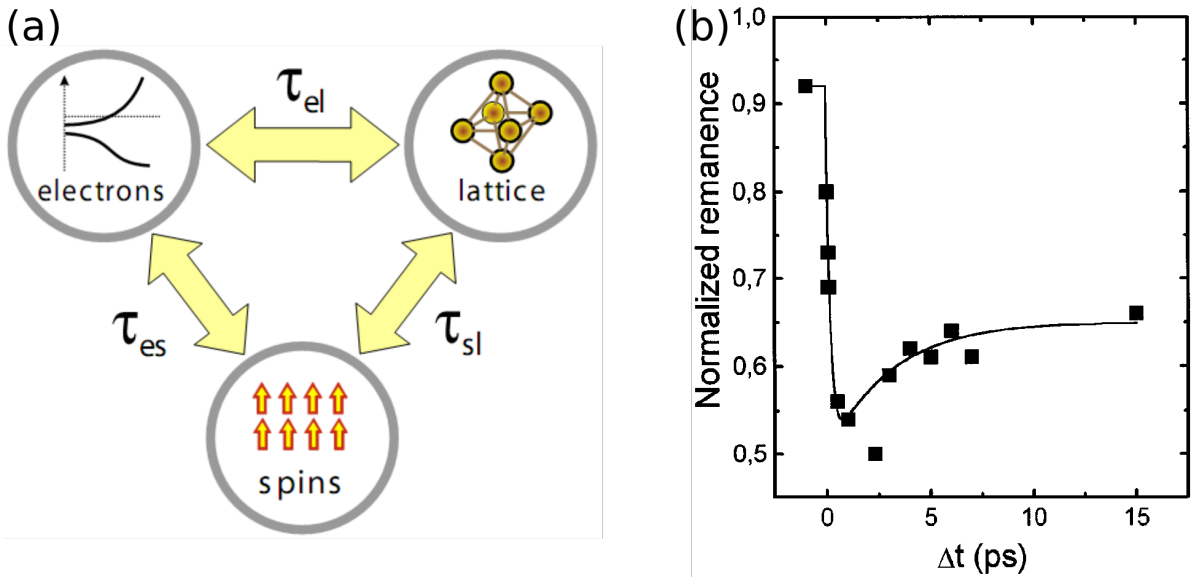

Figure 1.1.: (a) Schematic of interactions in ultrafast dynamics with characteristic time constants including the electron-lattice, electron-spin and spin-lattice [1]. (b) Transient remanent longitudinal MOKE signal as a function of time delay between optical pump and probe for a Ni film as reported originally by Beaurepaire, Bigot and co-workers [2].

probe. Often time, the signal given by one such event is too small and the measurements has to be repeated several time to achieve a sufficient signal to noise ratio, hence the stroboscopic part. This add the constraint that the system must get back to equilibrium between each pump probe event. By varying the delay and repeating the process, one can reconstruct the dynamic of a phenomenon. Both pump and probe can be realized by various physical means but they must be shorter than the time resolution required for the experiment. For ultrafast dynamics, the pump and the probe must be in the femtosecond range leaving very few physical process to choose from.

That's why pump and probe are usually realized by infrared (IR) pulses delivered by Ti:sapphire lasers. However, with the advent of suitable femtosecond sources, e.g. X-ray or XUV free electrons laser (XFEL) and high harmonics generation (HHG), the investigation of ultrafast magnetic dynamics has taken advantage of shorter probe wavelengths in the soft X-ray and extreme ultraviolet (XUV) range. Accessing this range has the following benefits:

- nanometre spatial resolution thanks to the very short wavelengths associated to this radiation [17];
- element specificity at energy resonant with absorption edges which allow to study different elements in a complex system and to compare their dynamics [18];
- few femtoseconds to attosecond time resolution to study the very early stages of light matter interaction and in our case light magnetization interaction [11];

- separating spin and orbital angular momentum contribution to magnetic dynamics to study the microscopic details of ultrafast magnetization dynamics [19].

In this manuscript, after a brief description of the experimental background, I will summarize some of the work I made in the field of ultrafast magnetization dynamics in the past 10 years using soft X-ray and XUV femtosecond sources. I will focus on the experiments made using X-ray resonant magnetic scattering (XRMS) which is a powerful tool to probe the magnetization at the nanoscale. I will also report on some of the technical developments I made to increase the possibilities of measurements at XFEL and HHG sources to study ultrafast magnetization dynamics. I will not develop other contributions such as ultrafast magnetization dynamics imaging [20, 21, 22] or HHG polarization control [23, 24].

The works presented here have been conducted with my colleagues at laboratoire de chimie physique – matière et rayonnement – Paris, France – (LCPMR) Jan Lüning (currently at Helmholtz Centrum Berlin), Emmanuelle Jal, Gheorghe S. Chiuzbăian, Romain Jarrier and Renaud Delaunay. It was also conducted as part of the PhD of my students Carla Alves, Alaa el dine Mehre and Xuan Liu and of the postdoctoral work of Marcel Hennes. The HHG experiments have been conducted in close collaborations with my colleagues at laboratoire d'optique appliquée – Palaiseau, France – (LOA) Philippe Zeitoun, Julien Gautier and Guillaume Lambert. The XFEL experiments benefited greatly from my collaborations with the group of Stefan Eisebitt (Max Born Institute in Berlin, Germany) and Christian David (Paul Scherrer institut in Villigen, Switzerland) and from collaborations with beamline scientists at the different XFEL in particular Marion Kuhlmann (DESY, Hamburg, Germany) and Flavio Capotondi (Elettra, Trieste, Italy).

2. Experimental background

2.1. Femtosecond XUV sources

2.1.1. High harmonic generation

Harmonic emission was first observed in 1961 using the newly developed ruby laser [25]. At that time, only the second harmonic of the 694.3 nm, 3 J, 1 ms laser could be generated in a quartz crystal with extremely low efficiency. 26 years later, the first HHG (the 17th order of a 248 nm laser) was observed [26]. This report was followed by an intense development of the field which aim at understanding the mechanism underlying HHG [27, 28] and at realizing a coherent light source in the XUV region delivering ultrashort pulses [29, 30]. In the past 20 years, the main focus of HHG related studies has been attosecond science [31, 32].

HHG can be understood at the atomic level by the so-called three steps model [27, 28]: (i) distortion of the atomic Coulomb potential of an atom due to the intense electric field of the focused laser is responsible for tunnel ionization of an electron; (ii) the electron wave packet is accelerated away from the atom by the laser electric field and when the electric field reverses (at a fixed point in space an electromagnetic field oscillates), it is accelerated back to the atom; (iii) the electron wave packet recombines with the parent ion when the field is nearly zero, leading to the emission of XUV radiation. To be able to detect this emission macroscopically and obtain a good conversion efficiency, the emission of all atoms has to be phase-matched (harmonics from different atoms must emit with the sampe phase) [33, 34].

Nowadays, HHG is a widely available source of coherent XUV femtosecond pulses since its principle is rather easy to implement. A high peak power laser (which are readily available commercially) is focused in a gas cell or gas jet filled with a gas (most often a noble gas) generating high harmonics (figrue 2.1). This principle has been used extensively to study atomic and molecular physics [35], before the advent of XFEL, and is still a powerful tool to conduct experiments in this field [36]. The wide spectrum delivered by HHG and the inherent synchronization between harmonics and the driving laser (allowing for jitter-free experiments) are also very appealing for the realization of ultrafast spectroscopy experiments in solids. However, the low conversion efficiency of the HHG process (at most 10^{-4}, typically 10^{-6}) make it a challenge to realize such solid state spectroscopy experiments. Nevertheless, in the recent years, clever experimental designs and progress in polarization control and polarimetry of harmonics have lead to very interesting results, particularly in the field of ultrafast magnetization dynamics [37, 17, 38, 39, 11].

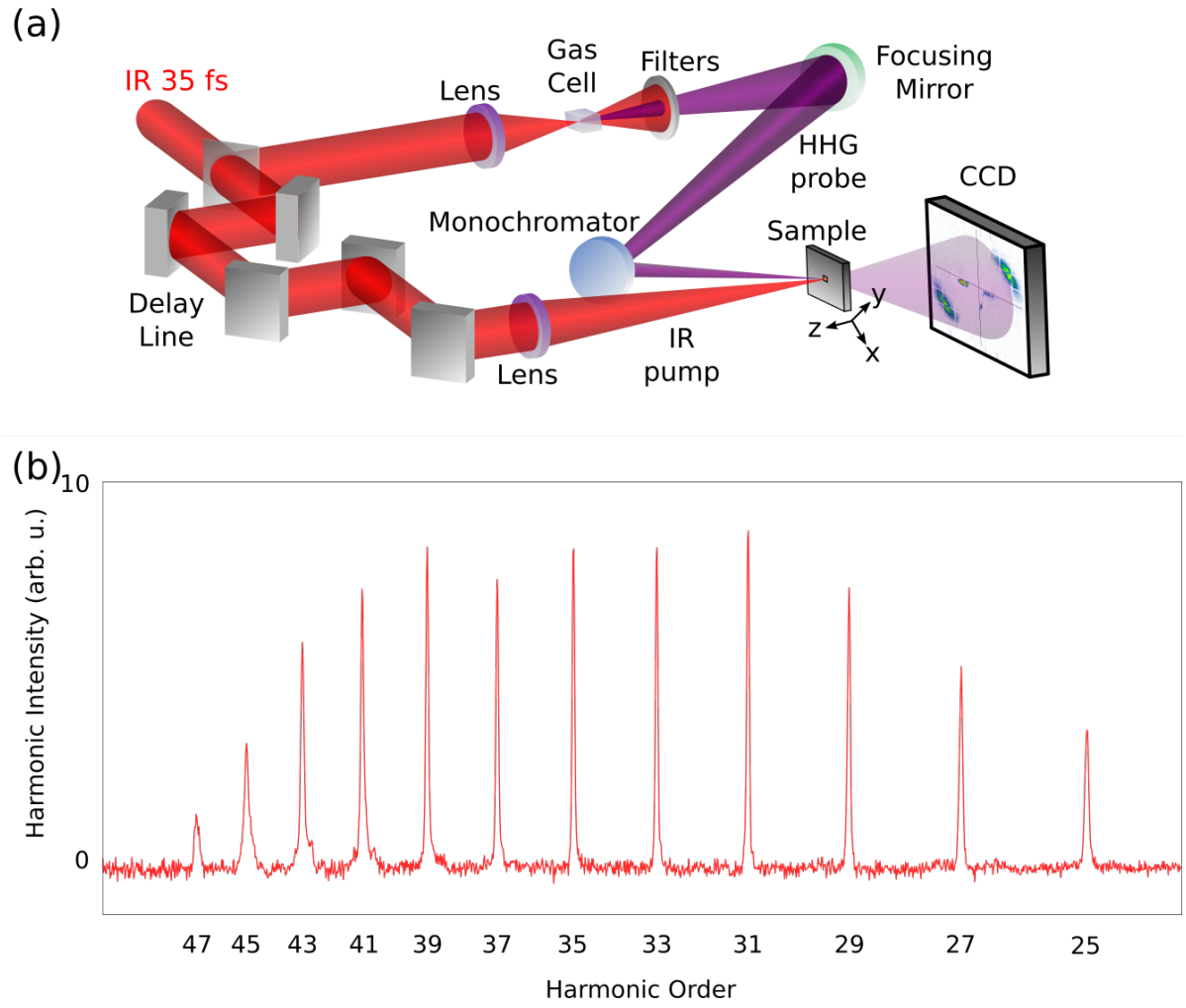

Figure 2.1.: (a) Typical high harmonics based pump probe setup. Femtosecond pulses from a Ti:sapphire laser (800 nm, 5 mJ here) are separated by a beam splitter. The main part is focused in a gas cell filled with neon generating (b) harmonic up to at least 47^{th} order. Higher harmonics are absorbed by the Al filter used to separate the harmonic beam from the driving IR light. After the gas cell the harmonics, here the probe, are focused onto the sample and can be monochromatized by a multilayer mirror. The second part of the beam is used to pump the sample out of equilibrium. A delay line on its path allow one to vary the delay between the pump and the probe.

2.1.2. X-ray free electrons lasers

XFEL are based on the radiation of an electrons bunch passing through an undulator (a periodic arrangement of magnets with alternating poles) [40]. The electrons are accelerated to close to the speed of light by a linear accelerator before entering the undulator where they emit X-rays or XUV radiations. Contrary to typical Synchrotron facilities based on electrons storage rings, the electrons bunch goes through the undulator only once before being dump. This allows for extreme compression of the electrons bunch and very short pulses of a few femtoseconds: coulombic repulsion between electrons does not have time to significantly lengthen the bunch.

The undulator are also usually significantly longer to allow the so-called self-amplified spontaneous emission (SASE) to kick in. At the entrance of the undulator, the electrons are evenly distributed within the bunch and they start to emit light. Interaction between this light and the electrons will be the cause of a structuration of the bunch called micro-bunching, each micro-bunch being separated by one wavelength from its neighbour. The emission of each micro-bunch being in phase with other micro-bunches, this will lead to an exponential increase of the radiation yield. Thus, the two main characteristics of XFEL sources are that they deliver very short and very intense pulses.

XFEL can either operates in SASE or be seeded. In SASE mode, in the first section of the undulator the electrons will produce spontaneous radiation. This initial radiation will serve as seed in the remaining part of the undulator. Consequently, this process is characterized by fluctuations in wavelength and pulse energy. This can be an issue for certain experiment but can be circumvented by using a seeding scheme. In seeding mode, an external laser pulse seeds the electron bunch from the start [41]. The pulse photon energy is then well defined by the seed and the intensity is more stable.

Free electrons LASer in Hamburg (FLASH) is the world's first XFEL delivering femtosecond pulses to users [42]. It is part of the research facility DESY (Deutsches Elektronen-Synchrotron) in Hamburg, Germany. User operation began in summer 2005. This is a SASE XFEL based on a superconducting linear accelerator which allows for long electrons bunch trains to be produced (up to 800 bunch/train) at a 10 Hz repetition rate. Today, the linear accelerator feeds two undulators lines FLASH1 and FLASH2 providing XFEL radiations for two experiments at the same time. FLASH1 has a fixed gap undulator and the wavelength is tuned by changing the electron energy from the accelerator while FLASH2 has a variable gap undulator and the wavelength can be changed in a wide range without influencing FLASH1. Both undulator delivers linearly polarized light. The photon energy range goes from 15 to 300 eV in the first undulator order and up to 800 eV in the third.

Free Electron Laser Radiation for Multidisciplinary Investigations (FERMI) is the XFEL source of the Elettra facility (Trieste, Italy). FERMI is a high gain harmonic generation XFEL [43]. It covers the same energy range as FLASH but it is the world's first seeded XFEL user facility. Contrary to FLASH, FERMI uses variable gap Apple II undulators which give users the ability to control the polarization of the emitted light on short time scales. Moreover, a multi-color mode was recently developed at FERMI [44]. This opens the field of the two colors experiments which we have already exploited

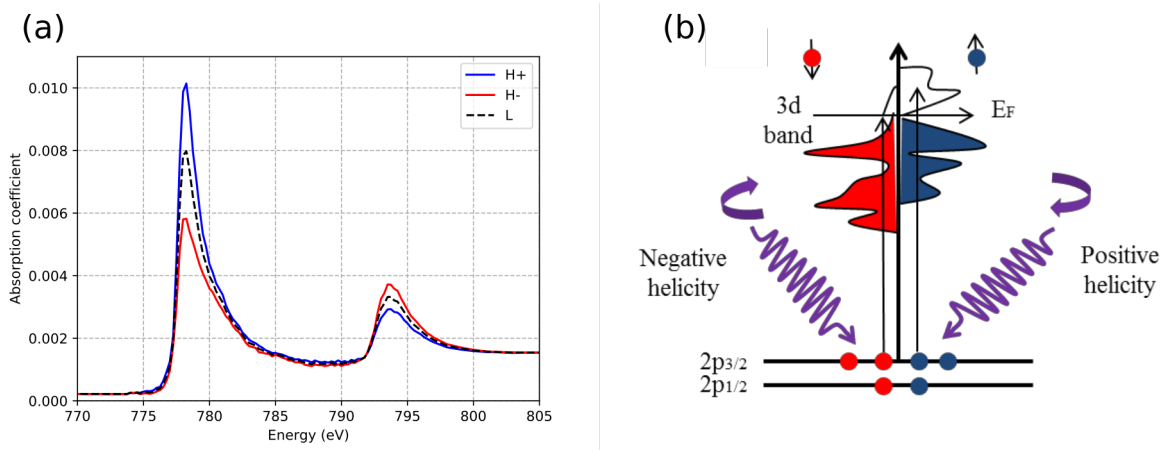

Figure 2.2.: (a) Absorption coefficient of magnetized Co as a function of energy around the L_3 ($\sim$ 778 eV) and L_2 ($\sim$ 794 eV) absorption edges for different light polarization, linear (L), right circular (H_+) and left circular (H_-). The magnetization axis of Co is parallel to the traveling direction of the light. (b) Simplified view of XMCD at the L edges of ferromagnetic transition metals [48]. At the L_3 edge ($2p_{3/2} \rightarrow 3d$), spin and angular momentum of electrons are parallel. Negative helicity photons will mostly excite majority electrons (spin down) which have very few states to transition to (optical excitation being spin conserving) and the absorption will be low. Positive helicity photons will mostly excite minority electrons (spin up) which have a lot of states to transition to and the absorption will be high. At the L_2 edge ($2p_{1/2} \rightarrow 3d$), spin and angular momentum of electrons are antiparallel, and XMCD is reversed.

for several studies [22, 45].

Linac Coherent Light Source (LCLS) is a SASE XFEL. It was the first hard X-ray XFEL opened for user operation (since 2009) [46]. Its energy range covers the $L_{2,3}$ edges of magnetic transition metals and $M_{4,5}$ of rare earth making it a great tool to study ultrafast magnetization dynamics with element selectivity. Since 2009, improvements such as two-colors generation or circular polarization [47] rendered this facility even more suited to such studies.

2.2. Resonant magneto-optical effects

2.2.1. X-ray magnetic circular dichroism

X-ray magnetic circular dichroism (XMCD) was first reported in the 1980s, following previous theoretical prediction for rare earth elements [49], in the pioneering work of Schütz and co-workers [50]. They observed that the absorption of a magnetized iron foil at that element K edge was different for right and left circularly polarized X-rays.

In the hard X-rays radiation range, XMCD was also observed at the $L_{2,3}$ of the rare earth elements Tb and Gd [51]. With the advent of soft X-ray synchrotron sources, similar reports were made at the $M_{4,5}$ edges of Tb and Gd [52, 53] and at the $L_{2,3}$ edges of nickel [54]. Shortly later, XMCD was also reported at the $M_{2,3}$ edges of transition metals [55, 56].

XMCD is particularly strong at the $L_{2,3}$ edges of the ferromagnetic transition metals Fe, Co and Ni. Figure 2.2(a) shows a typical XMCD spectra recorded at the Co $L_{2,3}$ absorption edges. For this $2p \rightarrow 3d$ transitions, XMCD can be qualitatively described by the so-called two step model [57] (figure 2.2(b)). In a first step, because of conservation of angular momentum, the circularly polarized X-ray beam transfer its angular momentum to the excited $2p$ electrons, in part to the spin since the $2p$ shell has a strong spin-orbit coupling. The excited electrons are thus spin polarized. In a second step, the exchange split $3d$ valence band acts as a spin detector for these electrons leading to an helicity dependent absorption. Since, the spin-orbit coupling is opposite for L_3 ($2p_{3/2}$) and L_2 ($2p_{1/2}$) edges, XMCD is reversed. Similar arguments can be made to explain XMCD at other absorption edges.

XMCD lead us to write the optical index for light of positive and negative helicity in magnetized matter as follows:

$$n_{\pm} = 1 + (\delta \pm \Delta\delta) - \imath(\beta \pm \Delta\beta) \tag{2.1}$$

where δ and β are the non magnetic dispersive and absorptive part of the optical index and $\Delta\delta$ and $\Delta\beta$ are magnetic corrections proportional to the magnetization of the sample. It has to be remarked that reversing the magnetization is equivalent to reversing the helicity.

An important feature of XMCD is that it allows one to separate the spin and orbital angular momentum contributions of magnetization thanks to the XMCD sum rules [57, 19].

2.2.2. Faraday effect

Michael Faraday was the first to successfully observe the effect of a magnetic field on the propagation of light through matter in 1845 [59]: when linearly polarized light goes through a magnetized material the polarization plane of the light will rotate and the beam will become elliptical rather than linear (see figure 2.3). This effect is strongest when the magnetization direction, or magnetic field, is parallel to the light propagation direction. Faraday effect can manifest itself over a very broad range of wavelengths in the electromagnetic spectrum but it is particularly strong at absorption edges which exhibit XMCD. It is particularly pronounced at the $L_{2,3}$ [60] and $M_{2,3}$ [61] absorption edges of Fe, Co and Ni.

Resonant Faraday effect can be fairly well understood as a consequence of XMCD. Indeed, a linearly polarized beam of light can be seen as the sum of two synchronized circularly polarized waves of identical intensities and opposite helicities. Since those two waves have different optical index, n_+ and n_-, they propagate differently in a magnetized

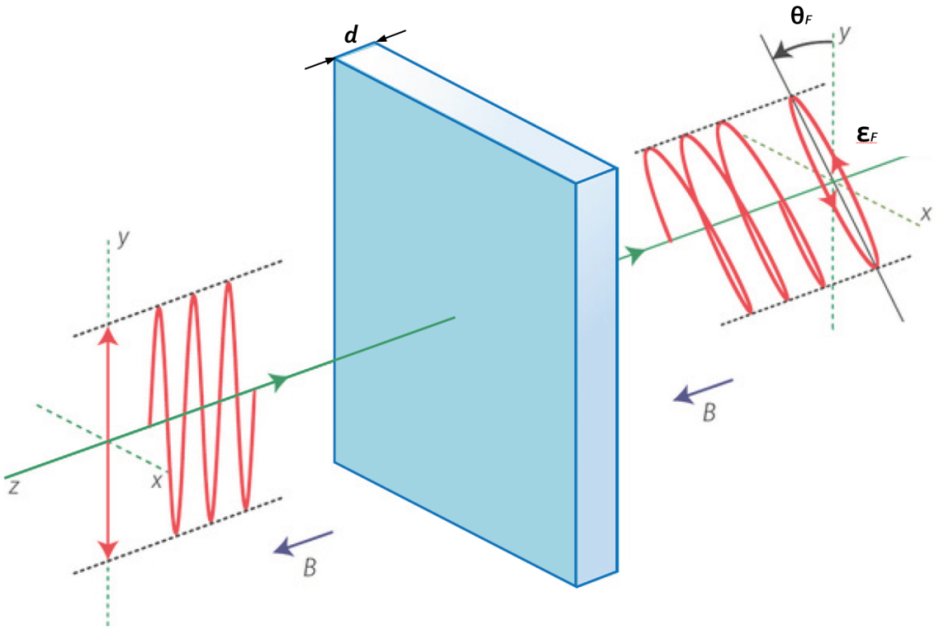

Figure 2.3.: Schematic representation of Faraday effect [58]. An incoming linearly polarized beam of light passes through a magnetized sample. After the sample, the polarization plane of the light is rotated compared to the incoming light polarization plane and the polarization becomes slightly elliptical. This rotation and ellipticity are respectively characterized by the so-called Faraday rotation, θ_F, and Faraday ellipticity, ϵ_F.

sample: (i) the phase shift between the two waves (due to $\Delta\delta$) leads to a rotation of the plane of polarization of the outgoing beam compared to the incoming beam; (ii) the difference in absorption between the two waves (due to $\delta\beta$) leads to the apparition of an ellipticity in the outgoing beam.

Faraday effect can be described in terms of two angle: the Faraday rotation, θ_F, and the Faraday ellipticity, ϵ_F (figure 2.3). For soft X-ray radiation (for example at the L edges of transition metals or M edges or rare earth), those two parameters can be shown to depend linearly on $\Delta\delta$ and $\Delta\beta$ respectively [62] for sufficiently thin films. This allow one to retrieve magnetization (which is proportional to $\Delta\delta$ and $\Delta\beta$) from the measure of either θ_F or ϵ_F. In the XUV region, at the M edges of transition metals, thing are a bit more complicated [61] but I recently demonstrated that one can design experiments which can retrieve the magnetization dynamics of the system [63].

2.2.3. Transverse Magneto-optical Kerr effect

Following Faraday works, John Kerr studied the effect of a magnetic field on the interaction of light with matter. In 1877, he discovered that upon reflection from a magnetized surface, the polarization state of linearly polarized light was modified in a way very similar to that of the Faraday effect [65]. This modification is called MOKE. There are

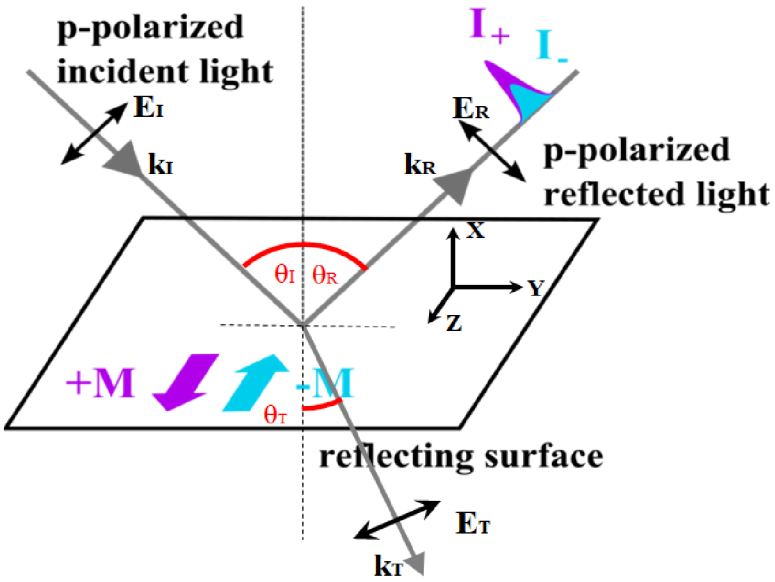

Figure 2.4.: Schematic representation of TMOKE [64]. An incoming linearly polarized beam of light (electric field E_I) is reflected from a magnetized surface. The polarization of the light is parallel to the plane of incidence (p-geometry) while the magnetization direction is perpendicular to that plane (transverse geometry) and parallel to the sample surface. Because of TMOKE, the intensity of the reflected beam (electric field E_R), I_+ or I_-, depends on the direction of magnetization of the sample, respectively M_+ and M_-.

three main MOKE geometries:

- perpendicular: the magnetization of the sample is perpendicular to the sample surface;
- longitudinal: the magnetization is parallel to the sample surface and to the plane of incidence;
- transverse: the magnetization is parallel to the sample surface and perpendicular to the plane of incidence (figure 2.4).

The first two geometries yield modifications of the polarization state of light while the TMOKE results in a change in intensity of the reflected light. More precisely, if we call M_+ and M_- the two magnetization states of the sample, the associated reflected light intensities, I_+ and I_-, will be different because of TMOKE. In the visible and IR range of the electromagnetic spectrum, TMOKE is very weak and the the perpendicular and longitudinal geometries are preferred to conduct experiments. That's why they are widely used to characterize the magnetic properties of various type of samples [66].

In the XUV range, the situation is very different. Indeed, resonant TMOKE can be a very strong effect [67] while transverse and longitudinal MOKE, albeit also enhanced, are

more difficult to measure since they require an XUV polarizer (which is not as trivially implemented as in the visible range). Consequently, the first femtosecond magnetization dynamic studies conducted with XUV radiations used a TMOKE geometry [37]. One has to keep in mind however that TMOKE is a surface sensitive effect: it probes the magnetization mostly in the first few nanometres of a sample. Another point to keep in mind while conducting TMOKE experiments is that the linearity between the signal and the magnetization is not guaranteed [68, 69].

2.3. Samples preparation and characterization

All sample studied in this report have been made by magnetron sputtering [70] mostly with the deposition chamber of the LCPMR. In magnetron sputtering, high energy ions from a plasma bombard a target made of the element one want to grow. The ions collisions with the target will result in the ejection of target material. A substrate is facing the target and ejected atoms will reach it and start to form a film. The total number of collisions increase in time and the atoms deposited on the substrate bind together stronger and stronger in tightly bound atomic layers.

Experimentally, a magnetron sputtering deposition machine consist of a few key elements. Inside a vacuum chamber (with a typical base pressure of 1×10^{-9} mbar), a cathode holding the target faces an anode where the substrate is mounted. A gas (most often argon) is then introduced into the chamber and a DC voltage is applied between the substrate and the target. A plasma is then formed inside the chamber and the magnetron sputtering process can start. A key parameter for the quality of the sample made is the deposition rate. It mostly depends on the gas pressure and on the high voltage power supply settings. All type of metallic monolayer, multilayer and alloy can be realized at LCPMR including magnetic films based on transition metals and rare earth elements.

Our primary characterization tool to control the quality of the magnetization layer is an optical MOKE setup [48]. It allows us to measure the magnetization hysteresis loop of the film which is characteristic of its magnetic properties. This setup is situated next to the deposition chamber and all samples are characterize immediately after realization. In addition to this optical setup, we have access to a magnetic force microscope to measure the magnetic structure of our films at the nanometer scale. We also sometimes perform X-ray reflectivity to control the different layer thicknesses of the films. If needed, additional characterizations are made using synchrotron radiation at SOLEIL.

3. Ultafast demagnetization at the nanoscale

3.1. Time-resolved X-ray resonant magnetic scattering

Before my experiments at the HHG source of LOA in the early 2010s [17], ultrafast demagnetization had not been studied at the magnetic domain level. This was due to the spatial resolution limit set by the IR laser wavelength of the ubiquitously used MOKE probe. Intuitively, this can be seen as a limitation on the available experimental data, because the particularities of an underlying magnetic domain structure can have an influence on macroscopic properties of a ferromagnetic material. Moreover, nanometre distances are the relevant length scale for energy and angular momentum transfer occurring on the femtosecond timescale between electrons, spins and the lattice, which are the processes underlying the macroscopically observed ultrafast demagnetization phenomenon.

To fill this gap we have studied a sample consisting of a $[\mathrm{Co}(0.4\,\mathrm{nm})/\mathrm{Pd}(0.6\,\mathrm{nm})]_{30}$ multilayer deposited by magnetron sputtering on a 30 nm thin Si_3N_4 multi-membranes (squares of $50\,\mu\mathrm{m}\times50\,\mu\mathrm{m}$) chip. This multilayer exhibits an out of plane magnetic anisotropy. The sample was demagnetized so as to present a a nanometric aligned stripe domain state with an in-plane oscillating magnetic field [71].

To probe the magnetization state of this sample, we used XRMS which provides element-specific statistical informations on the magnetic domain structure on the nanoscale [72, 73]. Due to the XMCD at the transition metals' M-edges, the optical index depends on the sample's magnetization (figure 3.1(a)). More precisely, the amplitude of the XMCD effect depends on the projection of the magnetic moment on the propagation direction of the incident radiation. This renders the presence of magnetic domain structures visible to the incident light, which is then scattered correspondingly (figure 3.1(b)).

It has to be noted that even linearly polarized light produces a scattering pattern. Indeed, linearly polarized light can be seen as the superposition of two circularly polarized components of opposite helicities. Each of those, will "see" the magnetic domain structure (albeit with an inverted contrast) and give the exact same scattering pattern (because of the Babinet's principle).

Like in any scattering experiment, statistical properties like size, form and contrast of the magnetic domains can readily be extracted from the intensities $I(q)$ of the scattering diagram, where the wave vector transfer q is proportional to the inverse of the spatial periodicity of wavelength d. We note that the integrated scattering intensity is related

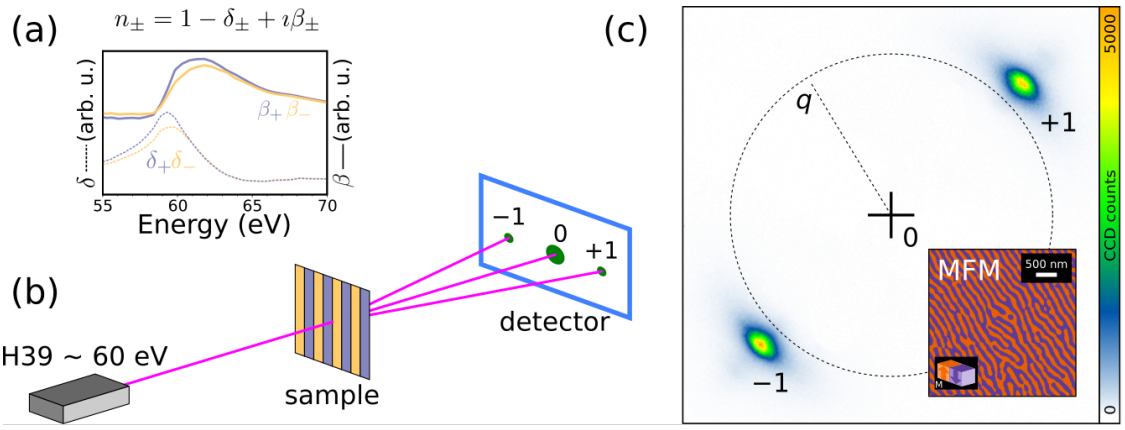

Figure 3.1.: Principle of X-ray resonant magnetic scattering shown at the $M_{2,3}$ absorption edge of Co. (a) Optical index of Co between 55 and 70 eV showing the differences between right and left circularly polarized light due to XMCD. (b) Because of these differences, a Co film with aligned nanometric magnetic domains acts as a diffraction grating for photons in resonance with the $M_{2,3}$ absorption edge (around 60 eV) and the incoming beam is diffracted into several scattering orders. (c) Measurement realized at the HHG source of LOA on a Co/Pd multilayer film presenting aligned magnetic domains with a period of about 150 nm. The magnetic domain structure shown in inset (magnetic force microscopy measurement) scatters the beam into a +1 and −1 diffraction order. The zero order has been blocked.

to the magnetization, M, itself. Hence, by following the time evolution of the integrated scattering intensity one can also study demagnetization dynamics in an experiment. The advantage of such an experiment is that no external field is required for saturating the sample's magnetization, which is a necessity in any study without spatial resolution.

In more details, the magnetic domain structure can be approximated by a square grating whose transmission alternates between t_+ and t_- for up and down magnetic domains (see inset of figure 3.1(c)). The diffracted intensity in the first order, I, of such a grating is given by [74]:

$$I \propto |t_+ - t_-|^2 \text{ with } t_\pm = \exp\left(\frac{2\pi\imath d n_\pm}{\lambda}\right), \tag{3.1}$$

where $n_\pm$, $n_\pm = 1 - (\delta \pm \Delta\delta) + \imath(\beta \pm \Delta\beta)$ is the optical index of up (+) and down (−) magnetic domains (equation 2.1), d the thickness of the film and λ the wavelength of the radiation. Developing expression 3.1, we find that I is proportional to $T(\Delta\delta^2 + \Delta\beta^2)$, where T is the average transmission of the grating. Given that $\Delta\delta$ and $\Delta\beta$ are both proportional to the magnetization M (see ref. [75]), it follows:

$$I \propto TM^2. \tag{3.2}$$

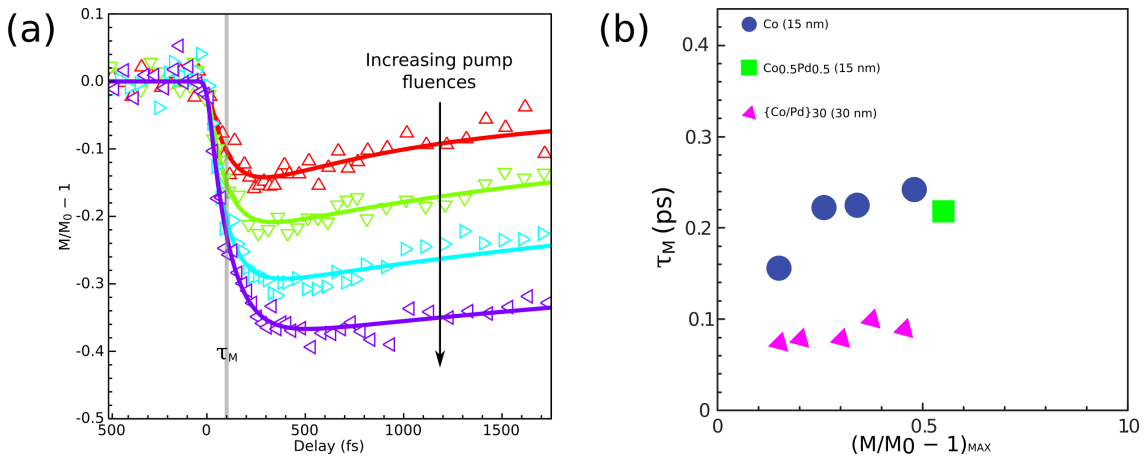

Figure 3.2.: (a) Normalized magnetization as a function of time delay recorded using XRMS with a monochromatized HHG source at about 60 eV on a Co/Pd multilayer for increasing pump fluences. This plots demonstrate that ultrafast demagnetization can be measured at the nanometre scale and is not a macroscopic effect. (b) Characteristic demagnetization time (pink triangle), τ_M, as a function of maximum demagnetization. τ_M is shorter than in previous reports for Co-based thin films (blue dots from ref. [1] and green square from ref. [19].) and does not increase with the amplitude of demagnetization as was previously reported [1].

The pump probe set-up (figure 2.1) is based on a Ti:sapphire laser ($\lambda_0 = 815$ nm), delivering 5 mJ, 40 fs full width at half maximum (FWHM), linearly polarized (horizontal) pulses at 1 kHz. Each pulse is split into a strong part and a weak part (pump) by a 90% – 10% beam splitter. The strong part is focused into a gas cell filled with neon (35 mbar) to generate high harmonics (probe) by non linear interaction between the laser and the gas. The generated harmonics retain the polarization of the infrared laser and span a wide photon energy range between 40 and 78 eV. Tuning the source parameters allows optimizing the efficiency for the generation of the 39$^{\text{th}}$ harmonic, which matches the Co $M_{2,3}$ absorption edges around 60 eV.

To suppress the incident infrared light, a 200 nm thick aluminum foil is introduced into the optical path. The transmitted harmonics are then focused (focal spot of 30 µm in diameter) by a spherical mirror coated with a wide band gap multilayer onto the sample. To select only the 39$^{\text{th}}$ harmonic, a second multilayer mirror, located a few centimetres before the sample, is used.

The pump beam goes through a delay line and is focused (focal spot of 150 µm in diameter) to excite the sample. The fluence of the pump beam can be adjusted and the size of the focal spot ensures a uniform illumination across one membrane. The harmonic light elastically scattered by the magnetic domain structure of the sample is collected by a PI-MTE CCD camera (Princeton Instrument) located 4 cm behind the sample and protected from any diffuse infrared light by an aluminum filter. The time resolution of this experiment is less than 45 fs (FWHM), which is set predominantly by

the infrared pulse duration (40 fs), since the harmonic pulses are much shorter [76, 77] and since there is no jitter between infrared and harmonic pulses in this setup.

The time-resolved images revealed that the magnetic domain structure remain globally the same throughout the demagnetization process: the spot positions and size remains the same for all delays (similar as in figure 3.1). However, the intensity of the spot change because of the demagnetization (equation 3.2). Figure 3.2(a) shows the magnetization (M normalized to the unpumped magnetization, M_0) as a function of time delay for a series of increasing pump fluences. The solid lines reproduce fits by a double exponential expression to the data (triangles), which allows us to extract parameters like the maximum demagnetization, the thermalization time (τ_{th}) and the relaxation time from the spin degrees of freedom to others ($\tau_{\mathrm{s-ph}}$) [19].

To obtain accurate values for $\tau_{\mathrm{s-ph}}$, long delay scans have been performed. The thermalization time can also be characterized [1] by the delay time τ_M at which the drop in magnetization reaches 63 % of its maximum . The values of τ_M are reported in figure 3.2(b). One notes that these values are fluctuating within 10 fs around 85 fs with no clear fluence dependence, although a slow increase with increasing fluence cannot be ruled out. A demagnetization of almost 45 % is achieved in the case of the highest fluence level used (11 mJ cm^{-2}), which is just under the destruction threshold of the sample in our repetitive kilohertz experiment. Nevertheless, even for this rather high degree of demagnetization, compared to other studies, we do not observe an increase of the thermalization time.

Our experiment revealed that locally, within each magnetic domain, the magnetization undergoes a rapid decrease, on the femtosecond timescale, as previously observed macroscopically for uniformly magnetized thin films. The overall magnetic domain structure, on the other hand, retains its organization, even for the highest excitation power accessible in this experiment. Surprisingly, the observed demagnetization times ($\sim$ 100fs) are shorter than those reported for uniformly magnetized Co compounds. Furthermore, they do not vary with excitation power as suggested by previous work.

3.2. Photonless ultrafast demagnetization

Around 2010, it has been proposed that the origin of ultrafast demagnetization could be due to spin-dependent motion of the optically excited hot valence electrons causing a spatial redistribution of the magnetization, either to an adjacent metallic layer [78, 12] or within the magnetic layer itself [79]. Strong experimental evidence for this so-called superdiffusive spin transport were reported [80, 81, 82, 83]. The question arose then whether these hot electrons could trigger ultrafast demagnetization without the need of a direct interaction of the pump optical beam and the magnetic layer.

To investigate this question [84], we implemented an IR-opaque capping layer on Co/Pd multilayers. The thin-film samples studied in this experiment have been grown by DC magnetron sputtering on 50 nm thin Si_3N_4 membranes. Two ferromagnetic [Co(0.4 nm)/Pd(0.6 nm)]$_{30}$ multilayer films were grown (figure 3.3(b)). One film was capped with a 3 nm thin Al layer to prevent oxidation of the magnetic multilayer. Since

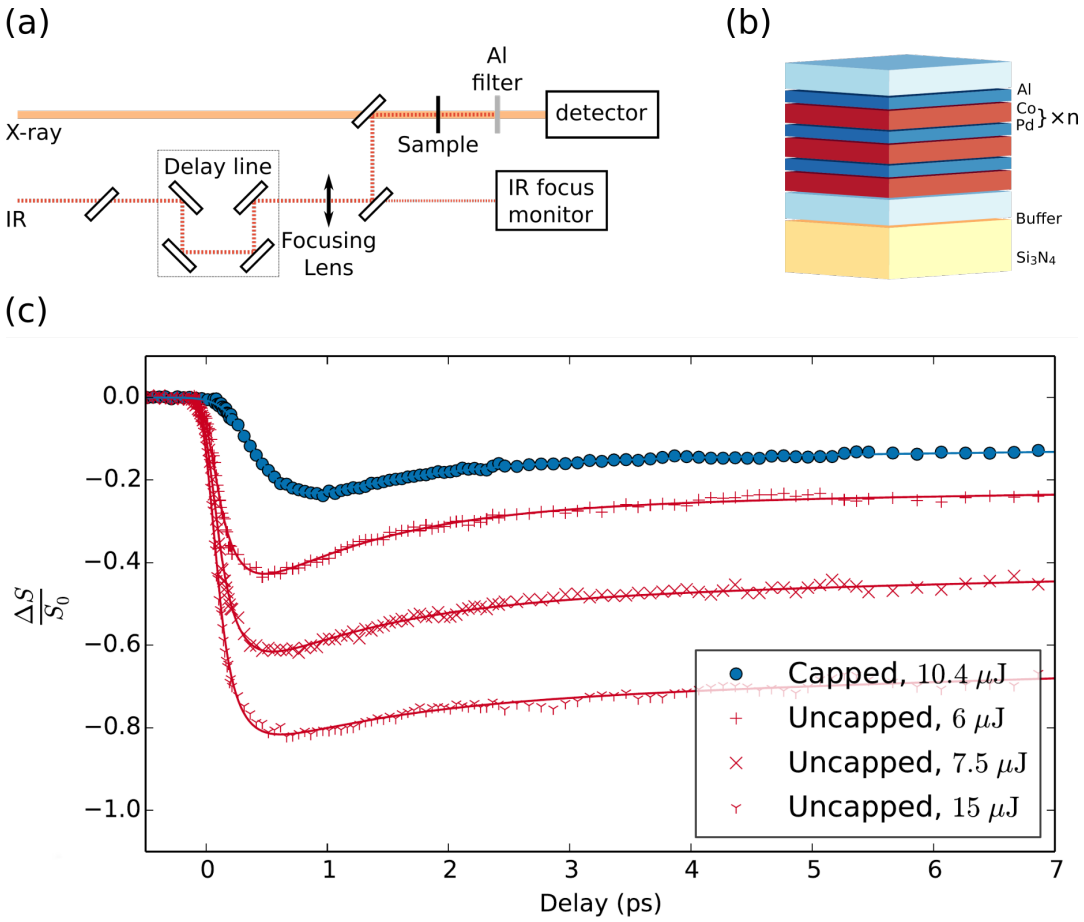

Figure 3.3.: (a) Schematic representation of the pump probe setup used at LCLS. (b) Composition of the Co/Pd multilayer sample (n = 30). The thickness of the Al cap layer is either 40 nm (capped sample) or 3 nm (uncapped sample). (c) Normalized scattering intensity as a function of time delay for capped and uncapped samples. The demagnetization of the capped sample is clearly delayed compared to the one of the uncapped sample, it is also a lot slower.

about 1.5 nm of this Al cap is instantaneously oxidized [85], we refer to this film as *uncapped* Co/Pd film in the following. This is in contrast to the *capped* Co/Pd film on top of which a 40 nm thick Al film was grown. Proper characterization of the number of photons reaching the magnetic layer demonstrates that the transmitted intensity is by orders of magnitude too small to excite the ultrafast demagnetization process for this latter film.

The experiment has been realized at the SXR instrument of the XFEL LCLS [86] equipped with the pnCCD camera [87] using XRMS as a probe technique for the temporal evolution of the local magnetization within the domains of the films (figure 3.3(a)). The 800 nm pump pulses triggering the magnetization dynamics were delivered by the femtosecond IR laser of the SXR end station [86, 88]. To uniformly excite the magnetic film on the 50 µm square membranes, a focusing lens (f = 75 cm) was positioned just

in front of the beamline's standard in-coupling mirror, which yields close to collinear beam propagation. The spatial beam profile and position of the IR pump beam was monitored during the experiment using an out-of-vacuum replica of the IR focus. Since the IR pulse length in the SXR hutch is about 50 fs, we chose a comparable X-ray probe pulse length. Both pulse durations are thus below the temporal resolution of the X-ray arrival time jitter correction, which sets the overall time resolution of the experiment to about 130 ± 20 fs [89].

As describe in section 3.1, we have employed XRMS as magnetization probe. Prior to the experiment, a demagnetization procedure with an oscillating, successively decreasing magnetic field oriented parallel to the film surface has been employed to obtain a magnetic domain structure of well-aligned stripe domains [71]. Tuning the X-ray photon energy to the magnetically dichroic Co L_3 edge (around 778 eV), this grating-like magnetic domain structure gives rise to localized scattering intensities corresponding to the grating's positive and negative diffraction orders. The intensity of these spots is measure as function of time delay to retrieve the magnetization dynamics.

The demagnetization dynamics of the uncapped Co/Pd film were excited with IR pump pulse energies of 20 µJ, 25 µJ and 50 µJ. Taking into account the reflectivity and absorption values, we can derive values for the IR absorbed energy : 6 µJ, 7.5 µJ and 15 µJ respectively, giving rise to a maximum degree of demagnetization at about 0.5 ps delay of 24 %, 38 % and 57 %. It has to be noted that this absorbed energy values might not correspond to the actual absorbed energy since the exact IR transmission through the transport line was not measured accurately. However, these values give us a very good relative scale to compare with the absorbed energy in the capped sample. Furthermore, the pump beam profile at the sample position was not measured with a sufficiently high accuracy to obtain an absolute fluence value. However, previous measurements on similar samples [17, 90] show that the fluences reached here should approximately be in the range of 5 to 15 mJ cm^{-2}.

In the case of the capped Co/Pd film, the IR pump pulse energy needed to be increased to 65 µJ to reach a demagnetization of 12 %. Taking into account the film's reflectivity and the layers' absorption, the IR photon pulse energy directly absorbed in the Co/Pd layer is estimated to be lower than 0.06 µJ. This corresponds to a fluence value within the focus area of 0.06 mJ cm^{-2}. Clearly, this amount of energy is more than one order of magnitude too small to trigger any noticeable demagnetization [90]. Within the 40 nm thick Al layer, on the other hand, 10.4 µJ are absorbed.

Scattering intensities of both films as function of time delay are reported on figure 3.3(c). On a first glance one notes that the magnetization exhibits in all cases the typical behavior associated with the ultrafast demagnetization phenomenon [2]: a drastic drop of the magnetization occurring on a sub-picosecond time scale, which is followed by a partial magnetization recovery taking place with a slower time constant on the order of one to a few picoseconds. On the other hand, the comparison of the two films reveals that the onset of the magnetization dynamics of the capped film is clearly delayed with respect to the one of the uncapped film. We note that this delayed onset is the expected signature of the demagnetization dynamics induced by the hot electrons generated by the IR pump pulse in the metallic capping layer.

By fitting the data [84], we estimate this delay to be about 270 fs. In addition, the comparison reveals a clear difference in the demagnetization rate, which is about a factor of two or so slower in case of the capped Co/Pd film. Interestingly, one notes that the dynamics of the partial recovery of the magnetization of the capped film is similar to the one of the weakly pumped uncapped film (6 µJ). This similarity indicates that about 400 fs after excitation of the magnetization dynamics, the nature of the excitation process itself does not influence the dynamics anymore.

In conclusion, we have demonstrated that ultrafast demagnetization does not require direct excitation of the ferromagnetic material by a photon pulse. In order to prove that affirmation we have measured the magnetization dynamics of a magnetic film capped by a thick Al layer. Contrary to pioneering previous work [83] the optical property of this capping layer have been thoroughly characterized and found to strongly absorb the IR pump pulse. The remaining photon pulse reaching the underlying magnetic film is three orders of magnitude too weak to trigger the demagnetization observed. Comparison between the dynamics of this capped film with the ones of an uncapped reference film showed that the onset of the demagnetization dynamics is delayed and the initial loss in magnetization is slowed down. These observation are compatible with a demagnetization process triggered by a flux of hot valence band electrons from the Al cap layer to the underlying magnetic film. The mechanism by which these hot electrons trigger the demagnetization remains to be elucidated.

3.3. Multi-sub-latices magnetization dynamics

Part of the difficulty to quantify the importance of superdiffusive spin transport [12] mentioned in section 3.2 comes from the fact that one must measure the hypothetical magnetization transfer to the metallic layer from the magnetic layer. Measuring the magnetization of the metallic layer is at best tricky at worst impossible. For example, in the initial system studied by Battiato and co-workers [12], a nickel film on aluminium, there is no easy way to quantify the magnetization of the Al layer.

To circumvent this difficulty, we chose to study a sample with an easier design: a Co/Pt multilayer system. Indeed, the magnetization of the Co and Pt layers can be probed selectively by using photons in resonance with the Co $M_{2,3}$ (around 60 eV) and Pt N_7 (around 71 eV) absorption edges to investigate the ultrafast demagnetization process of these two elements [22].

According to the model of superdiffusive spin transport [12], spin-polarized electrons will be generated by the pump pulse and then transport part of the magnetization from the Co layer to the Pt (figure 3.4(a)). The magnetization of the Co layers should then decrease similarly to a single element film while the magnetization of the Pt layers should increase (figure 3.4(b)). Other process could blur this clear cut view but we should at least be able to see different magnetization dynamics for Co and Pt.

To realize this experiment, we have perform XRMS on a $[Co(0.6\,nm)/Pt(0.8\,nm)]_{20}$ multilayer grown on a 50 nm thin Si_3N_4 membrane. The main difference with the experiment described in section 3.1 is the fact that we focused all the harmonics onto the

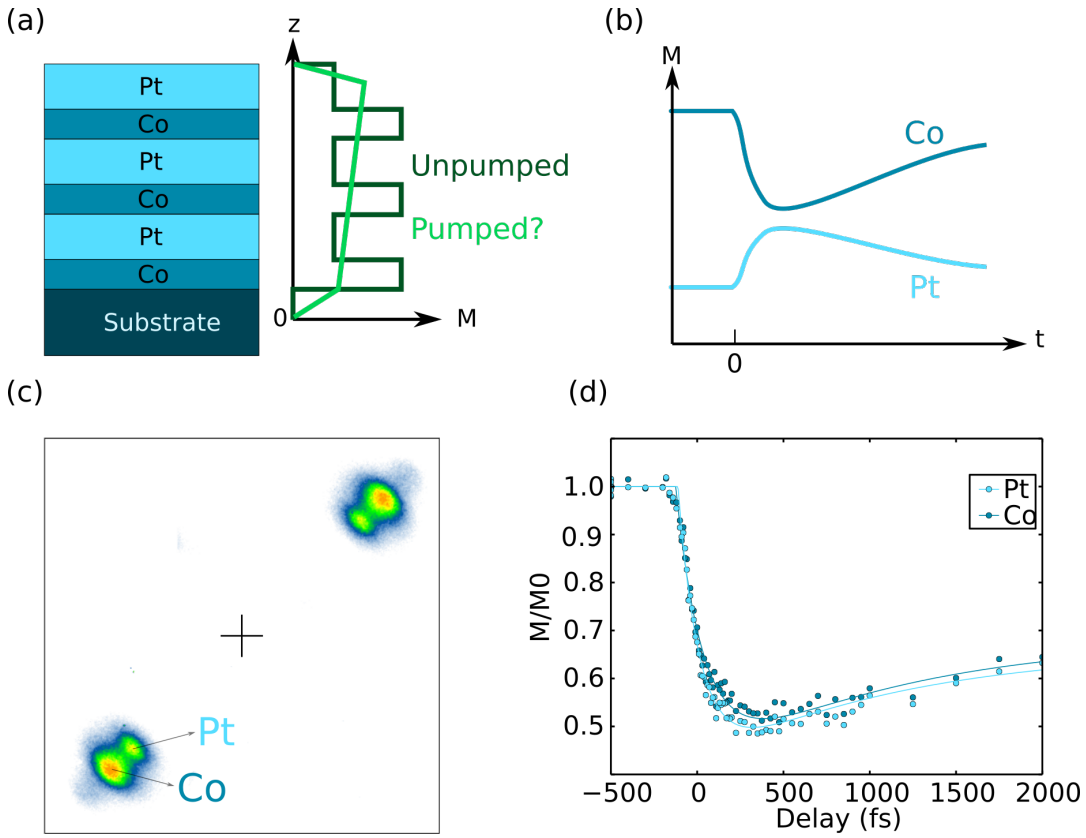

Figure 3.4.: (a) Schematic representation of a Co/Pt multilayer sample and the associated magnetization profile (Unpumped). Following the theory of superdiffusive spin transport [12], after the pump part of the magnetization of Co should be tranfer to Pt and the magnetization profile should become more uniform (pumped). (b) The magnetization dynamics of Co should show the usual dip while the one of Pt should show a bump (or at least a slower decrease). (c) XRMS obtained for a Co/Pt sample with aligned magnetic domains. There is no monochromator and all the harmonics are focused onto the sample. This leads to scattering spots for harmonics in resonance with the Co $M_{2,3}$ edges (largest central spots) but also for harmonics in resonance with the Pt N_7 (inside spots) and O_3 edges (outside spots) [22]. (d) Normalized magnetization as a function of time delay as measured with photons in resonance of the Co and Pt edges. Both dynamics are very similar revealing that the transfer of magnetization from Co to Pt is at most very weak.

sample. Indeed, we have replace the spherical mirror by a toroidal mirror in grazing incidence and we have remove the monochromator. We now have harmonic in resonance with both absorption egdes of interest.

Figure 3.4(c) shows the scattering obtained in this configuration. We have now three scattering spots on each side of the detector corresponding to the Co $M_{2,3}$ edge (central

most intense spots), to the Pt N_7 edge (inner intense spot) and also the Pt O_3 edge. By following the intensities of these spots as a function of time delay, we can retrieve the magnetization dynamics of Co and Pt. The transients are shown in figure 3.4(d). Even though Pt demagnetizes slightly more, the two magnetization dynamics are almost identical.

In conclusion, it does not appear that a significant magnetization transfer from the Co layers to the Pt layers occur in this system. However, it has to be noted that in this type of multilayer, Pt has a strong magnetization induced by the neighbouring Co atoms. This could prevent us to see small superdiffusive effect under a larger demagnetization of Pt. To circumvent this problem, we have crafted a cleaner experiment and realized it at the XFEL FLASH to have more photon at the Pt edge.

The experiment is the following. Instead of using a Co/Pt multilayer we use a Co/Pd multilayer of the same composition as the ones described in sections 3.1 and 3.2. This multilayer is grown on a few nanometers thick Pt buffer layer and cap with a Pt layer of the same thickness. The Pt layers are only in contact with Pd layers to prevent any initial magnetization of Pt. With this new design, it should be easier to pick up any magnetization transfer towards the Pt cap or buffer layer. The experiment is realized using XRMS in transmission. We were not able to demagnetize the sample a lot but we could not detect any significant transfer of magnetization to the Pt layers confirming our previous results.

3.4. Ultrafast magnetic anisotropy dynamics

Since our first study on magnetization dynamic of magnetic thin films with strong perpendicular magnetic anisotropy (PMA) and presenting alternating domains with "up" and "down" magnetization [17], there have been several report on the magnetization dynamic on similar system. For example, Pfau and co-workers [80] studied Co/Pt multilayers at the Co $M_{2,3}$ absorption resonance and found an ultrafast shift of the maximum value of the scattering intensity with a time constant of approximately 300 fs, which they attributed to a superdiffusive spin-current-induced domain wall broadening. In a similar experiment, Zusin and co-workers scrutinized CoFe/Ni multilayers at the Ni L_3 edge and identified a pump-induced shift of the diffraction ring reaching 6 % within 1.6 ps which they interpreted as an ultrafast domain dilation, resulting from in- elastic electron-magnon scattering [91]. This contrasts our earlier work where the magnetic domain structure remained unaffected during the ultrafast demagnetization process [17]. These examples clearly illustrate the need to conduct additional studies in order to (a) further quantify the impact of ultrashort laser excitation on magnetic thin films with a complex spin texture and (b) clarify the role played by superdiffusive spin currents when changes in the magnetic structure occur on femtosecond timescales.

To do so we have perform a time-resolved XRMS experiment on a 50 nm thick amorphous $Co_{88}Tb_{12}$ sample grown on 50 nm thick Si_3N_4 membranes. After deposition, the samples were subjected to a demagnetization procedure using an oscillating in-plane field with decreasing amplitude to obtain a nanometric magnetic domain structure. The

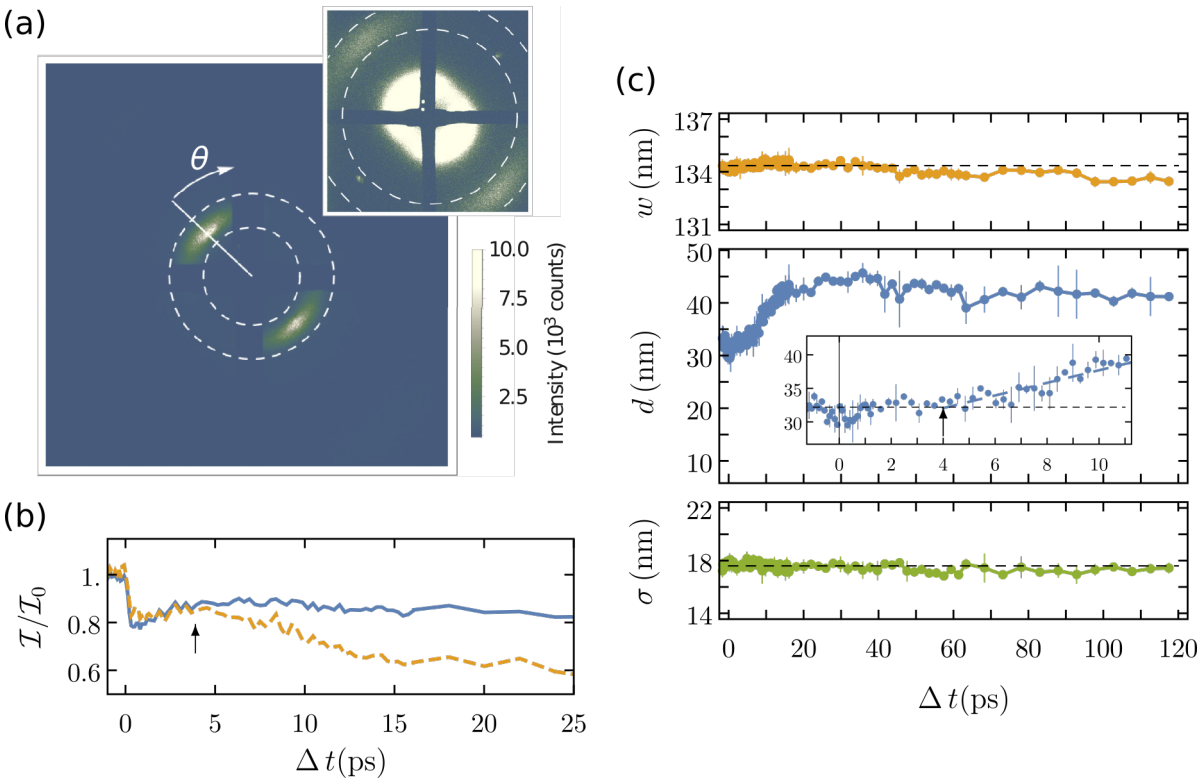

Figure 3.5.: (a) XRMS of a $Co_{88}Tb_{12}$ presenting aligned stripe domains showing the first an third order scattering spots. (b) Normalized scattering intensity as a function of time delay for first and third scattering orders. After about 4 ps the two dynamics begin to diverge revealing a modification of the magnetic structure. (c) Domain size, w, domain wall linear width, d and domain size distribution, σ as a function of time delay. The dynamic of these parameters is retrieved by fitting the XRMS data to a linear domain wall model [71]. The domain wall width increase after 4 ps while the other two parameters remain constants over time.

particularity of this study is the fact that we were able to observe the $\pm 3^{rd}$ scattering orders in addition to the $\pm 1^{st}$ orders that we usually follow to measure the magnetization dynamic [92]. The scattering pattern is shown in figure 3.5(a). These additional informations allow us to retrieve the average period, w, of the magnetic domain structure as a function of time but also the average domain wall width, d.

A first analysis of the data can be done by simply integrating the intensity of the $\pm 3^{rd}$ and the $\pm 1^{st}$ magnetic scattering orders and by plotting this intensity as a function of time delay. The results of such an analysis are reported on figure 3.5(b). It can be clearly observe that after 4 ps the dynamics at the 3^{rd} and 1^{st} orders diverge: the 3^{rd} orders intensity drops in comparison to the 1^{st} orders intensity.

To link this drop to meaningful physical parameters we have fitting our data to the model of magnetic domain structure proposed by Hellwig and co-workers [71]. This

model considers the aligned magnetic domain structure as a trapezoidal grating with linear domain wall. Three parameters can be retrieved from the model: the average period of the grating, w, the average linear domain wall width, d, and the size distribution of the domain size, σ. The evolution of these parameters as function of time delay is shown of figure 3.5(c). Only the d change over time. After 4 ps it starts to increase from about 30 nm to about 45 nm (around a delay of 20 ps). After that it relaxes slowly to its initial value.

It can be shown be a detailed analysis [92] that the change of domain size is the result of a modification of PMA. However, the time scales observed may not reflect the characteristic time scales of modification of PMA itself. Indeed, our observation could be affected by the finite spin reorientation times within the domain wall itself which could be of the order of several picoseconds considering the typical propagation speed of spin waves.

4. Technical development to measure ultrafast magnetization dynamics

4.1. "Single shot" magnetic dynamic recording

Typically, experiments resolving ultrafast processes rely on repetitive pump probe techniques that do not allow probing of phenomena having a stochastic nature or systems that are difficult to reset repeatedly to the initial state. To overcome these limitations, various methods based on spatial and spectral encoding of the pump probe time delay have been developed in optical spectroscopy, which allow for time reconstruction of an ultrafast process from a single optical laser pulse [93, 94, 95].

In the X-ray range so far, a single X-ray or XUV pulse from XFEL succeeded only in capturing the transient state of a sample at a single time delay [20], with the notable exceptions of multiple split and delay setups sampling a few discrete time delays at once [96]. In the following, a novel experimental method that makes it possible to continuously probe with a single femtosecond XFEL pulse the response of a system to an ultrafast excitation over an extended time interval [97].

Our experimental technique, to which we refer to in the following as XUV streaking, is based on a basic principle of diffractive zone plate optics. Each zone of the zone plate diffracts light to the focal point adding a delay of λ/c per zone, where λ is the wavelength of the XUV pulses and c is the speed of light. The optical path length from a zone plate to its focal point is the shortest for rays diffracted from the innermost zone of the zone plate and it increases continuously with the radial distance from the zone plate centre (figure 4.1(a)). When a single probe pulse illuminates the zone plate, it is diffracted into a continuous set of sub-pulses that converge at the focus. As each sub-pulse propagates along a different path, each of them reaches the focus at a different time and with a different angle. Their propagation continues after the focus, and the sub-pulses separate again, reaching spatially distinct locations, e.g., on an area detector. In this way the arrival time of each sub-pulse to the focus is encoded into the spatial coordinates on the detector. When a sample is placed in the zone plate focus, these sub-pulses probe the sample at different times, e.g., with respect to the arrival of an external pump pulse exciting the sample. The time evolution of the sample properties is thus encoded in the image recorded by the area detector. The choice of an off-axis illumination of the zone plate [98] is ideal to separate the different diffraction orders and to maximise the accessible time delay window for a given beam size.

XUV streaking also overcomes a limitation of conventional pump-probe experiments at unseeded XFEL. The stochastic nature of SASE results in strong fluctuations of XUV

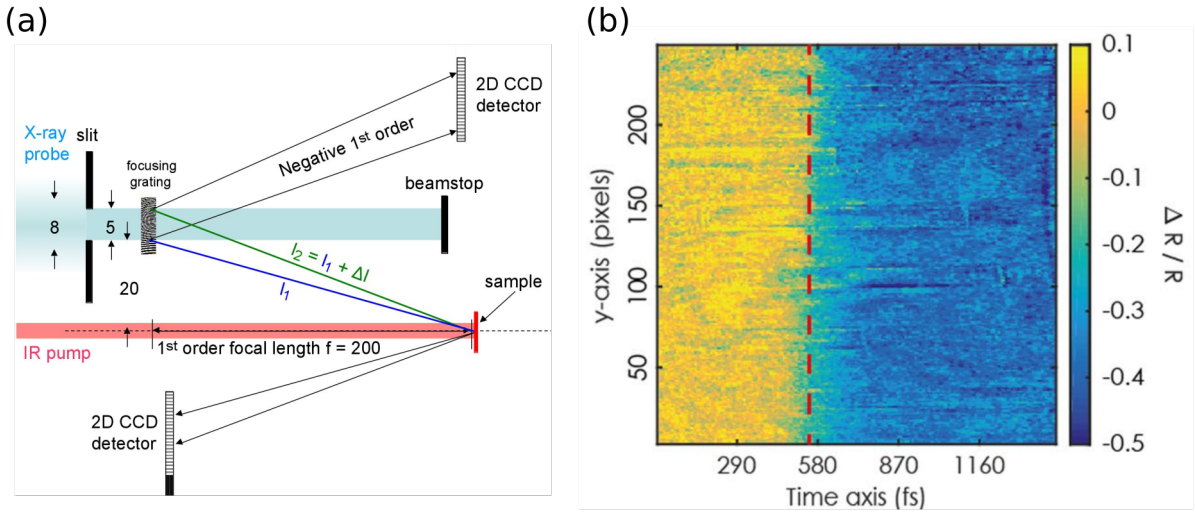

Figure 4.1.: (a) Schematic representation of single shot magnetic dynamic recording. The incoming XUV beam passes through an off-axis Fresnel zone plate. The path from the inner part of the zone plate to the focal spot is shorter than the path from the outer part introducing a time delay between rays that passes at this two positions. For the entire beam, there is a continuous range of delays between these two extreme. A sample is situated at the focal position of the beam which then diverge and is recorded on a 2D detector where time is encoded in space. The negative first order of the zone plate is also recorded on a 2D detector to normalize the data. (b) Normalized image obtain for a Co thin film pumped with an IR pulse showing the correspondence between space and time. The change in color along the horizontal axis is due to ultrafast demagnetization of the Co film.

pulse parameters such as arrival time or spectral composition [99, 100]. As conventional pump-probe measurements require averaging over many XFEL pulses, such fluctuations result, for example, in a deterioration of the achievable energy and time resolution. Retrieving the full time evolution of the ultrafast response of the sample using a single XUV pulse avoids the need of averaging over a series of XXFEL pulses, and allows approaching the achievable energy and time resolution given by the characteristics of a single XFEL pulse. As the whole dynamics of an ultrafast process is captured in a single pump-probe event, XUV streaking gives access to the ultrafast dynamics of stochastic phenomena and irreversible phase transitions in materials. Note that this is even useful when repetitive pump-probe measurements are possible, since capturing the entire trace at once allows selecting specific probe pulses, which can improve the data quality.

To demonstrate the capabilities of our novel XUV streaking technique we investigated the ultrafast demagnetization dynamics occurring in a thin ferromagnetic Co film (20 nm in thickness capped with 3 nm of Al grown on Si substrate) upon non-thermal excitation by an intense, femtosecond short IR pulse. Since up to now, all the experiments on ultrafast demagnetiwation have relied on repetitive pump probe techniques, it remains an

open question whether this phenomenon is indeed governed only by a single reproducible mechanism, as commonly expected, or whether multiple pathways, characterised by different demagnetization dynamics, are present.

To gain sensitivity to the transient magnetic properties of the sample we employed resonant TMOKE. The XUV photon energy was tuned to the cobalt $M_{2,3}$ edge (around 60 eV, corresponding to a wavelength of 20.8 nm) and the sample oriented close to its Brewster angle. In this experimental configuration a change in the sample magnetisation generates a variation in XUV reflectivity of up to 40 %. The unfocused FLASH pulse is used to illuminate the $4.8 \times 4.8\,\mathrm{mm}^2$ Fresnel off-axis zone plate. The $+1^{\mathrm{st}}$ diffraction order beam is focused on the area of the sample excited by the IR laser pulse. The sample reflects the beam towards a high sensitivity two-dimensional detector (reflection detector). The -1^{st} diffraction order beam is divergent and goes directly to a second two-dimensional detector (reference detector). We employ the reference detector to account for shot to shot fluctuations in the intensity profile of the XFEL beam, as well as inhomogeneities in the illumination and diffraction efficiencies of the zone plate.

To experimentally quantify the transient magnetization change induced by the IR laser pulse (fluence of $15\,\mathrm{mJ\,cm^{-2}}$), we collected reflectivity measurements using single XFEL pulses. After correcting for illumination fluctuations and after rescaling the image to the calculated time delay (given the zone plate characteristics), we obtained images such as the one presented in figure 4.1(b). The demagnetization of the film is clearly seen as a change of reflectivity of the sample over time. The red dashed line represent roughly the time overlap between the pump and the probe. By averaging the image along the y-coordinate, one obtains the single shot time resolved reflectivity curve shown in figure 4.2(a). We note that the signal-to-noise ratio of these single shot data is excellent, well comparable to what has been obtained so far by averaging over a large number of pump-probe events in repetitive pump-probe measurements [17].

Figure 4.2(b) shows the statistical distribution of the spin relaxation time τ_M obtained by fitting (with a double exponential expression [97]) the time resolved reflectivity curves recorded for each of 193 consecutive events. The measurements follow a unimodal distribution, and the fitting of the experimental histogram with a Gaussian distribution shows an excellent agreement leading to a value of $< \tau_M >$ of 113 ± 20 fs, in excellent agreement with the value obtained in a single pump probe event. We note that this value is comparable with our experimental time resolution of ~ 120 fs and that within this limit, we do not observe a multimodal distribution peaked around more than one value that could indicate that the magnetic system followed different paths on each demagnetization event. This observation illustrates that, within our time resolution, the evolution of the ultrafast demagnetization process is truly deterministic.

Since resonant TMOKE provides a very strong magnetic dichroism (see above), it was ideally suited for a first feasibility demonstration. On the other hand, this experimental geometry can only be employed to study the magnetization dynamics of the surface of a sample in materials exhibiting an in-plane magnetization. To demonstrate a broader applicability of the XUV streaking technique, we used the XMCD effect in transmission to follow the magnetization dynamics of Co at $M_{2,3}$ edges in 50 nm thin $Co_{76}Dy_{24}$ alloy films grown on 30 nm thin Si_3N_4 membranes exhibiting out-of-plane magnetization [101].

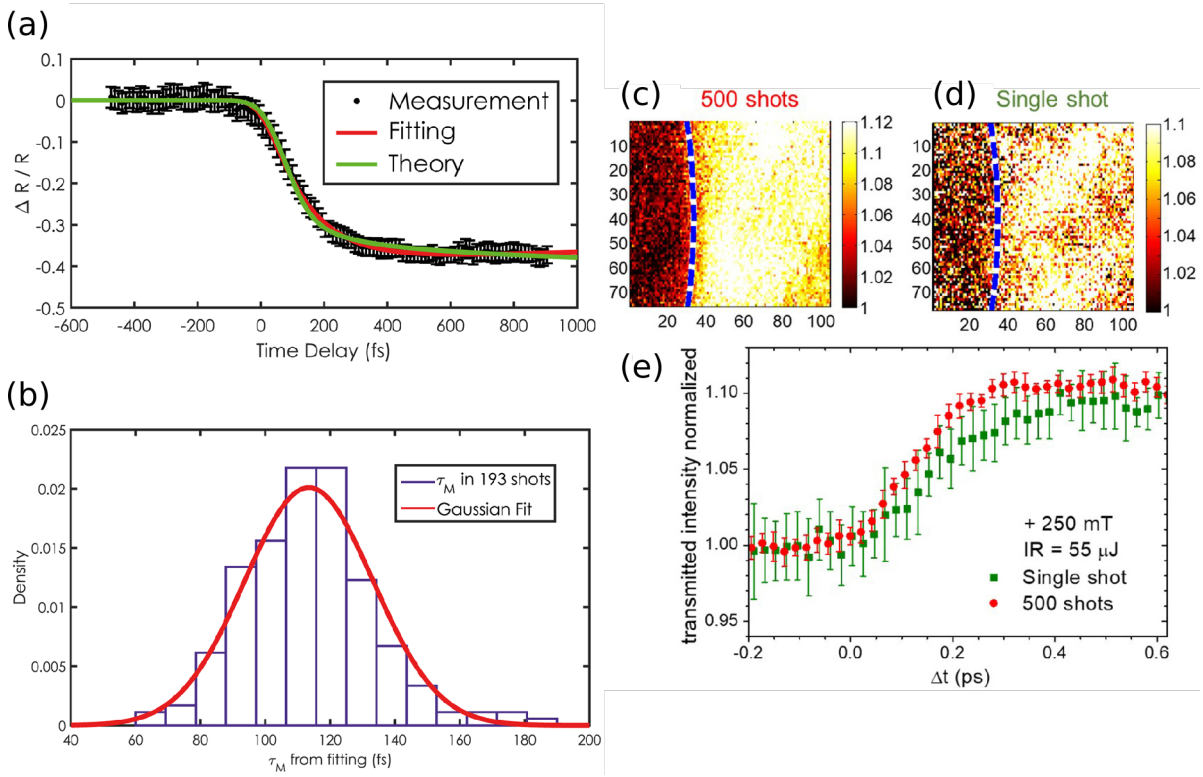

Figure 4.2.: (a) Normalized reflectivity (TMOKE geometry) as a function of time delay obtained after exciting a Co thin film with a femtosecond IR pulse recorded with a single shot XFEL pulse. The transient is obtained by integration along the vertical axis of the image of figure 4.1(b) and can be fitted with a double exponential expression to extract the demagnetization time, τ_M. (b) Distribution of demagnetization times, τ_M, obtained for 193 single shot magnetization dynamic recordings. Normalized image recorded for (c) multiple and for (d) single XUV shots showing the demagnetization transient of a $Co_{88}Dy_{12}$ thin film after excitation by a femtosecond IR pulse. The magnetization of the film is probed by XMCD in transmission. (e) Integration of previous two images showing the intensity as function of time delay. The signal to noise ratio of the single shot transient is already good but recording several hundred shot enhance significantly the data quality allowing one to study very weak effect.

The experimental setup is very similar that the one describe above except that the XFEL beam goes through the sample instead of being reflected. The experiment was conducted at the beamline DiProI of FERMI since we need circularly polarized XUV light to conduct an XMCD experiment. A permanent magnetic field of $\pm 250\,\mathrm{mT}$ is applied to reset a single domain state after each pump probe event. Figure 4.2(c) (d) and (e) shows the results obtained. In the corrected images (figure 4.2(c) and (d)), the magnetization dynamic is clearly visible for multiple shots recording as well as single

shot recording. This is particularly impressive since, contrary to TMOKE, the XMCD contrast is rather weak (at most 10 % here). The integration of these images along the vertical axis (figure 4.2(e)) confirm this impression. The single-to-noise ratio is good for single shot data and very impressive for multiple shots recording. The ability to use XUV streaking with low contrast probe demonstrated here will open up new measurements possibilities in the field of magnetization dynamics and beyond.

4.2. X-ray pump X-ray probe: towards few femtoseconds time resolution

At XFEL recent developments now allow for the generation of few femtoseconds X-ray pulses [102, 103] which have the potential to yield more versatile time-resolved spectroscopic experiments. Unfortunately, the traditional IR pump X-ray probe experimental schemes are typically limited by the pulse duration of the IR laser, typically between 30 and 100 fs at XFEL facilities. The arrival time jitter between IR and X-ray pulses further degrades the time resolution. It has to be noted that schemes have been developed at XFEL to produce several X-ray pulses separated by a variable delay to perform X-ray pump X-ray probe experiments [7,8,9] [104, 44, 105]. These approaches have the advantages of getting rid of the jitter and of being theoretically only limited by the duration of the X-ray pulses. They also offer the powerful possibility to excite core electrons and can hence trigger dynamics that differ from those generated by IR lasers. Unfortunately, those methods rely on XFEL special operation modes and are not widely available for users. Moreover, they have some limitations such as the range of delays accessible (typically between zero and a few hundreds of femtoseconds).

Our goal is to fully exploit the very short X-ray pulses delivered at XFEL in an X-ray pump X-ray probe geometry to obtain a sub-15-fs time resolution with an easy-to-implement user-side setup [106]. This is realized by splitting the X-ray beam into two parts: the first part is used to excite the sample and the second part is used to probe the sample state. In that way, we are only limited by the X-ray pulse duration. This enabled us to study the onset of the magnetization dynamics in Ni film with the best time resolution achievable at XFEL. In the following, we describe the split and delay setup that we have designed, installed, and commissioned at FLASH.

Our experimental setup (see figure 4.3) relies on a split and delay unit consisting of a flat rectangular mirror ($120 \times 20\,\mathrm{mm}^2$), a fused silica ultra-flat substrate, and two spherical mirrors (focal length of about 1500 mm). The flat mirror (splitting mirror) is set at a grazing angle of 1.4° and geometrically splits the incoming beam (16 mm in diameter) into two parts. A major part of the XFEL intensity passes the mirror and reaches the first spherical mirror (pump mirror) which focuses the beam onto the sample: this constitutes the pump beam (purple). The reflected part reaches the second spherical mirror (probe mirror) and is also focused onto the sample: this constitutes the probe beam (orange). The angle between the two beams is 2.8°. Both pump and probe mirrors are coated with a wide band aperiodic multilayer coating purchased from optiX

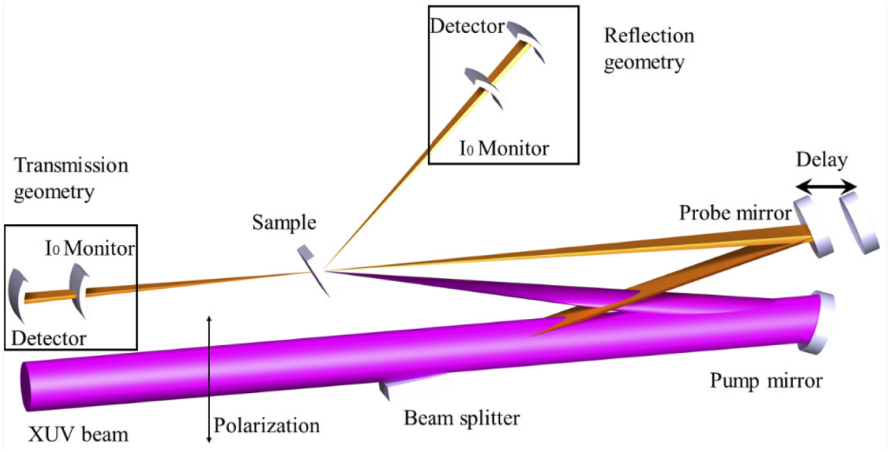

Figure 4.3.: (a) Schematic representation of the split and delay setup. The incoming XUV beam is separateid in two parts by a fused silica substrate at grazing incidence (beam splitter). The main part, the pump (purple), passes along the substrate and is focused by a spherical mirror set at a near normal incidence onto the sample. The reflected part, the probe (orange), is also focused onto the sample by a near normal incidence spherical mirror. This mirror is mounted on a motorized stage and a time delay can be introduced between the pump and the probe by moving this stage. The probe beam is recorded after the sample either in reflection or transmission geometry. Both spherical mirror are coated with a wide band multilayer.

fab. (Jena, Germany) , reflecting XUV radiation with at least 15 % efficiency in the 52 eV to 67 eV photon energy range.

We keep the pump mirror fixed and control the spatial overlap by vertical and horizontal tilts of the focusing probe mirror. The position of the two beams is monitored by imaging the X-ray induced fluorescence of an yttrium aluminum garnet (YAG) screen positioned at the sample position with a CCD camera. In order to ensure that the two beams remain overlapped during the experiment, vibrations have to be kept at a minimum. Indeed, if we want to keep the positions of the two beams within 10 µm of their initial positions, the variations of the angle of incidence on each mirror has to be maintained below 10 µrad. This is achieved by using a low vibration design for the mirror mounts and by isolating the vacuum chamber from any vibration source, especially from the vacuum pumps.

The time delay is changed by moving the probe mirror. The motorized stage used for this motion is set parallel to the probe mirror to sample direction: the properties of spherical mirrors ensure that the probe beam position remains stable while varying the delay. Moreover, the small alignment variations which may arise while scanning the delays can be corrected by the motorized rotations of the probe mirror (a correction table is recorded before the measurement). Since the beam impinges on the spherical mirrors at near normal incidence the delay changes amount to $2 \times \Delta l/c$ where Δl is the position of the probe mirror compared to the zero-delay position and c the speed of

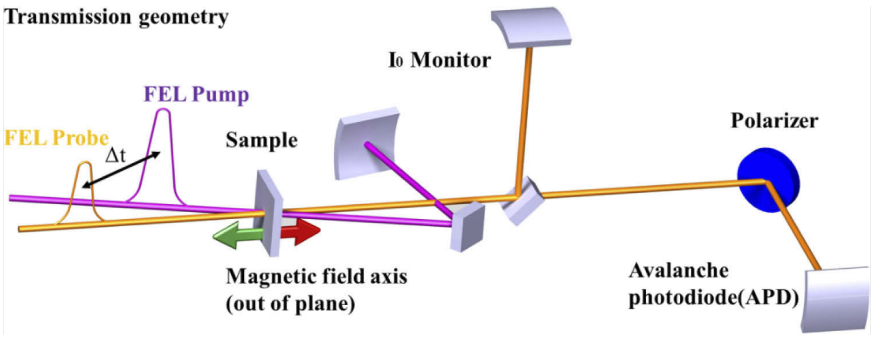

Figure 4.4.: Details of the transmission geometry detection scheme. The sample is magnetized out of plane by a set of permanent magnets. After the sample, the probe beam goes through a beamsplitter (a thin Si_3N_4 membrane). The reflected part is measured by an APD and is used as intensity monitor. The remaining part is used to measure the Faraday rotation induced by the sample magnetization thanks to a multilayer coated polarizer and an APD. The intensity of the pump beam is also recorded allowing us to sort the data by pump fluence.

light.

The probe beam can be focused down to a 50 µm spot, FWHM, on the sample and the size and pointing variations are negligible over the complete range of delays (about 10 ps or 1.5 mm). To homogeneously pump the sample, the pump beam focal spot has to be larger, about 100 µm, FWHM. This is easily achieved by using the mirror with the longest focal length for the pump. Indeed, the tolerance on the mirror curvature being of the order of 1 %, there is a few millimeters difference between the focal lengths of the two mirrors. The profile of the beam also allows us to estimate roughly the pump fluence on the sample by taking into account the reflectivity of the different elements in the system. We can achieve a pump fluence of at most 2.5 mJ cm^{-2} which is sufficient to demagnetize the different samples with an incoming XFEL pulse energy as low as 10 µJ. Contrary to IR pump schemes, there is almost no reflectivity and 50 % to 90 % of the pump is absorbed by the magnetic layer (depending on its thickness and the exact photon energy).

Since the XUV pulses at FLASH2 are linearly polarized, it is impossible to use XMCD directly, even though it is the preferred X-ray technique to probe magnetization in transmission. We therefore employ the resonant Faraday effect as a probe of the magnetization state of the samples. We have recently demonstrated how to measure femtosecond magnetization dynamics using the Faraday effect at photon energies in resonance with absorption edges of elements [63]. The configuration of the experiment is sketched in figure 4.4. For this experiment, we have studied a 30 nm thin Ni sample. It was sputter deposited on chips consisting of a nine-by-nine grid of 50 nm thick Si_3N_4 windows. The windows are squares of 50 µm. The samples have been capped by a 5 nm Al layer to prevent them from being oxidized.

In transmission geometry, the sample is set at normal incidence and magnetized out

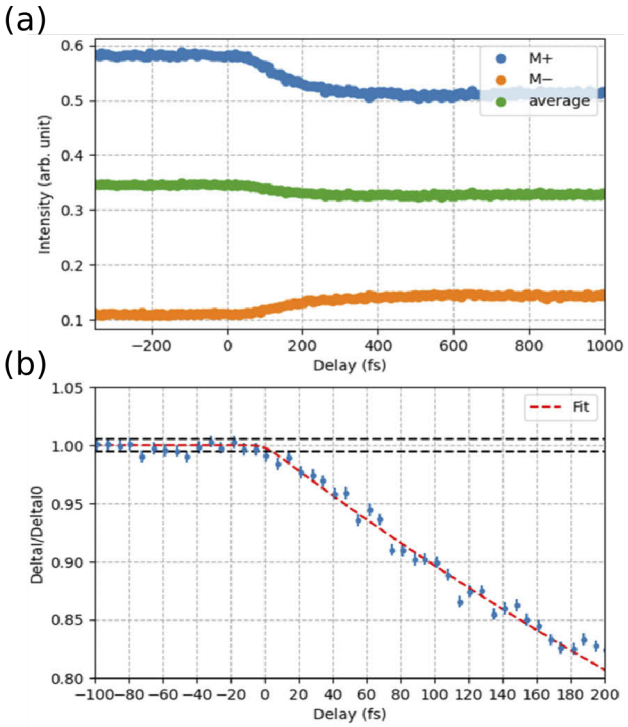

Figure 4.5.: (a) Normalized intensity recorded after the polarizer as a function of time delay for opposite magnetization direction and for an Ni film excited with an XUV pulse. The green curve (in the middle) is the average intensity. (b) Magnetization as function of time delay as obtain by taking the difference of the two precedent transients and normalizing by the average value before pump (negative delays). This curve as well as the fit and the dashed line showing the standard deviation of the unpumped signal reveal that the time resolution is better than 15 fs.

of plane by permanent ring magnets (maximum field of 350 mT , high enough to saturate the magnetization of the samples) to maximize the Faraday effect. To reverse the direction of the magnetic field, we use two sets of permanent ring magnets mounted in opposite direction on a vertical motorized stage. Behind the sample, the pump and probe beams diverge. The pump beam intensity is recorded on an X-ray photodiode after reflection on a gold coated mirror.

Part of the probe beam is reflected upwards by a Si3 N4 window and recorded by an APD. This window is set to an angle of incidence of 45°, close to the Brewster angle, and only reflects the p-component of the beam. Since the Faraday rotation is of the order of a few degrees at most, the p-component of the beam is mostly unaffected by the magnetic state of the sample, allowing us to measure the probe beam intensity even when the sample is excited by the pump. The fact that the I_0 monitors for pump and probe are placed after the sample provides a high precision since only the intensity of the light passing the 50 µm apertures of the sample is measured.

After the Si_3N_4 window, the probe beam is reflected by the polarizer which consists

of a few repetitions Al/B4C multilayer mirror with a reflectivity higher than 10 % in the 55 eV to 66 eV energy range also purchased from optiX fab. This polarizer mostly reflects the s-component of the electric field of the XFEL pulses (the s-reflectivity is at least 200 times higher than the p-reflectivity), and its intensity is measured by an APD. The angle of incidence of the polarizer can be adjusted to optimize the amplitude of the magnetic signal by maximizing the extinction ratio (ratio between s and p reflectivity).

The polarizer can also be rotated around the probe beam axis in order to move the reflection out of the horizontal plane. This allows us to work slightly out of the p-geometry which is essential to be able to see a difference between the two directions of magnetization [63]. Indeed, since the polarizer and detector are only sensitive to the magnitude of the s-component of the beam, both directions of magnetization give the same signal in a pure p-geometry. Working slightly out of the horizontal plane results in different signals for the two different magnetization directions, the difference between the two being proportional to the magnetization of the sample [63].

Figure 4.5(a) shows the normalized transmitted intensity as a function of pump probe time delay recorded for the Ni film for opposite direction of the sample magnetization. The time-resolved magnetization, M, is proportional to the difference between these two signals ΔI [63]. There is clearly a magnetization dynamics induced by the XUV pump. The sum of these two signals is not a straight line revealing a weak non-magnetic dynamic. Figure 4.5(b) shows this signal normalized to the unpumped difference, ΔI_0 . From this measurement, we can estimate a total time resolution of better than 15 fs for our experiment by looking at the initial drop of magnetization. Indeed, this drop occurs in an interval of 12 fs (three consecutive points each separated by 6 fs) showing that we can determine the onset of demagnetization with a precision better than 15 fs.

Furthermore, fitting the graph of figure 4.5(b) with expression for demagnetization dynamics found in [78] for example, we can determine the best Gaussian envelope describing the time resolution ($\Gamma(t)$ function in [78]) of our data: the best results are obtained for a Gaussian with a 10 fs FWHM. Finally, the estimated pulse duration of less than 10 fs would yield at worst a time resolution of about 14 fs (the convolution of two 10 fs Gaussian profile is a 10 times square root of 2 Gaussian profile). All these evidences point to a sub-15 fs time resolution in this experiment. This time resolution is not far from the best time resolution achievable at attosecond harmonic sources – about 5 fs [11] – and the best that has yet been achieved for a femto-magnetism experiment at XFEL.

5. Conclusion and outlook

5.1. Summary

In the past ten years, my work in the field of ultrafast magnetization dynamics has lead to several interesting new insights, thanks to the unique abilities of XUV radiation to probe the magnetic state of a sample more accurately than optical MOKE. Among those achievements I would like to point out the first observation of ultrafast demagnetization at the nanometer scale [17], the first report of ultrafast demagnetization driven only by hot electrons [84] and the observation of the PMA dynamic in transition metal rare earth alloy [92].

Furthermore, with my colleagues at LCPMR and collaborators in Switzerland, Germany and Italy, we develop the technique of "single shot" magnetic recording. This technique is very powerful either as a tool to study non reproducible dynamic [97] or as a mean to achieve unprecedented data quality thanks to a very high sampling rate [101, 45, 107]. It will undoubtedly have application beyond magnetization dynamics but in this field it could for example be coupled with our XUV pump XUV probe scheme to study subtle effects such as optically induced spin and orbital momentum transfer [11].

My work has also opened a few questions that I want to investigate in the next few years. In the following, I describe two future projects.

5.2. Ultrafast dynamic of electronic structure

Since the first ultrafast magnetization dynamics experiment using soft X-rays, it has been observed that ultrafast electronic effects could modify the absorption spectra already at few hundreds of femtoseconds after excitation [108] and that this effect persists to some extent after 50 ps [109]. Although these modifications are small, they could have an impact on the magnetization dynamics [110] but a systematic experimental investigation of this relationship remains to be done. Theoretical modeling of this phenomenon has been scarce [110, 109] and no consensus has emerged on the origin of this effect.

In the XUV range, it has been demonstrated that very high excitation fluences could lead to a spectacular modification of the magnetic scattering form factor and related scattering intensity and the associated resonant magneto-optical effects close to the absorption edges [111]. However, the proposed explanation, based on energy shifts of the absorption edge in the very early stages after an excitation, has been partially revised in view of more recent works considering stimulated emission [112, 113] or onset of ultrafast demagnetization [114].

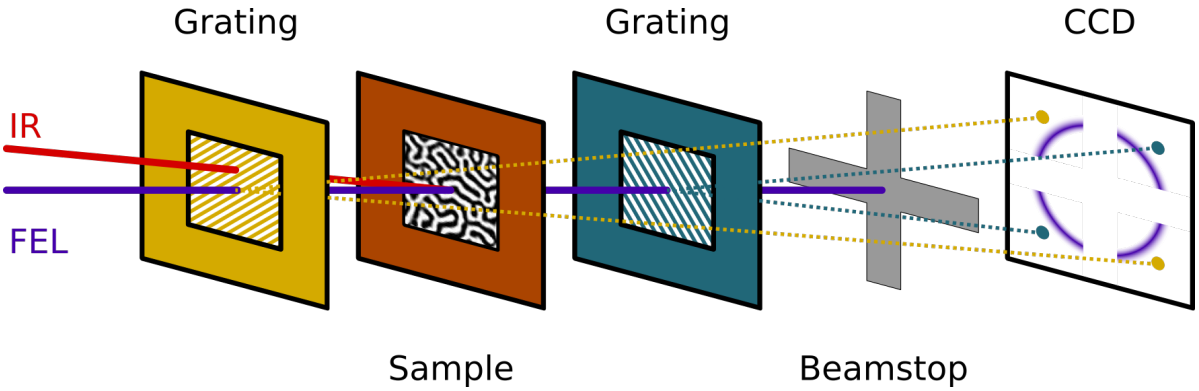

Figure 5.1.: Schematic description of the transient transmission dynamics experiment. The XFEL beam passes a first normalization grating before reaching the sample where an IR femtosecond pulse has pushed the system out of equilibrium. After the sample, the beam is scattered by a second grating which will be used to measure the transmitted intensity before being blocked by a beamstop. All the diffracted signals are recorded at different positions on a CCD camera.

In comparison to previous reports [108, 109, 111], our recent observation of a strong laser-induced ultrafast modification of the electronic system, revealed by the sharp increase in absorption of a Ni/Cu/Fe thin film for photon energies close to the Ni absorption M edge is then surprising [45]. Indeed, the 15 % change in absorption (XAS) clearly dominates the few percent modification of XMCD which in addition is delayed compared to the electronic response. Moreover, it occurs for low fluences (only a few $\mathrm{mJ\,cm^{-2}}$) and is strongly dependent on the probe energy [107]. Our observations could be explained by a shift of about 500 meV of the absorption edge, significantly more than what has been observed at the L edge (130 meV) [108].

Our goal will be to ascertain the existence of this shift, measure its amplitude and understand its origin by performing systematic measurements and theoretical modeling. This work will be conducted at the HHG source of LOA and at the XFEL FERMI and FLASH and we will have collaboration with Prof. Dr. Hubert Ebert at LMU (Munich, Germany).

As a first step to study this aspect of ultrafast dynamics in solids, I proposed and recently realized the following experiment at FERMI (see schematic representation on figure 5.1).We have studied a studied a Co/Pt multilayer presenting a nanometric magnetic domains structure which scatters the incoming FEL beam in a ring. The intensity of this scattering pattern allows us to retrieve the magnetization as explained in section 3.1. In order to measure the transmission variations of the sample, which are linked to the transient variations of the electronic structure, we placed a diffraction grating after sample. The characteristics of this grating are calculated to give a diffracted intensity of the same order as the intensity diffracted by the magnetic structure. To enhance the signal to noise ratio, we placed a similar grating before the sample (rotated by 90° compared to the back grating). The diffracted orders of this grating pass through the

sample but are not excited by the IR pump laser. Consequently, they are directly proportional to the incoming intensity and are used to normalize both the time-resolved magnetic scattering and transmission signals. After the back grating the direct beam will be blocked by a beamstop while the diffracted photons will be collected by the same CCD camera ensuring the best linearity possible between the different scattering patterns. It is not possible to record directly the transmitted beam since the dynamic range of the CCD camera is not high enough. Indeed the transmitted beam and the magnetic scattering have very different intensities.

The data recorded are still under analysis but the idea is to reproduce this experiment at the $M_{2,3}$ absorption edges of Co and on different ferromagnetic elements.

5.3. Magnetization dynamics in embedded nanopillars

The ability to control the magnetization of magnetic materials without applying large magnetic fields is a strong, technologically relevant, motivation in the quest for new hybrid (nano) materials. Ideally, such systems should afford the possibility to control the magnetization fast and with reduced energy consumption. In recent years, hybrid systems consisting of heavy metals associated with $3d$ ferromagnetic metals for current-assisted magnetization switching [115] and multiferroic materials for electric-field-control of magnetization [116] have been intensively studied. However, the fastest control of magnetization can be achieved with light. All optical switching [13] has recently emerged as a powerful technique to steer the magnetization on femtosecond timescales, but it is not yet clear to what extent it applies to nanostructures.

Consequently, it would be interesting to follow a new path in manipulating magnetization by combining hybrid systems development and optical magnetization control (see figure 5.2). This approach would rely on the elaboration of new vertically assembled nanocomposites (VANs) made of magnetic nano-objects epitaxially embedded in photostrictive (PS) thin films. PS materials respond to light irradiation with a deformation of their lattice [117]. The interest in PS materials has been renewed following recent reports of huge light-induced strains (up to 2 %) that can be generated on short timescales (down to the few picosecond range) in $SrRuO_3$ and $SrIrO_3$ [118, 119] thin films with thickness in the tens of nanometers range.

While the possibility to couple magnetic thin films with PS materials has been demonstrated, the classical planar architecture is problematic: magnetic thin films must be very thin because of light absorption and strain relaxation issues. One possibility to circumvent this problem is to switch to other types of geometries. VANs are made of nanopillars of a given material that are embedded epitaxially in a thin-film matrix. These nanocomposites are mostly grown using pulsed laser deposition (PLD). Using a ferromagnetic material for the nanopillars allows one to obtain assemblies of nanomagnets whose size (diameter in the 2 to 10 nm range) and magnetic anisotropy can be tuned [120, 121]. The control of the magnetic anisotropy is a direct consequence of the nanoarchitectures that give rise to large axial strain.

Our research hypothesis is that it should be possible to elaborate optimized, epitaxial,

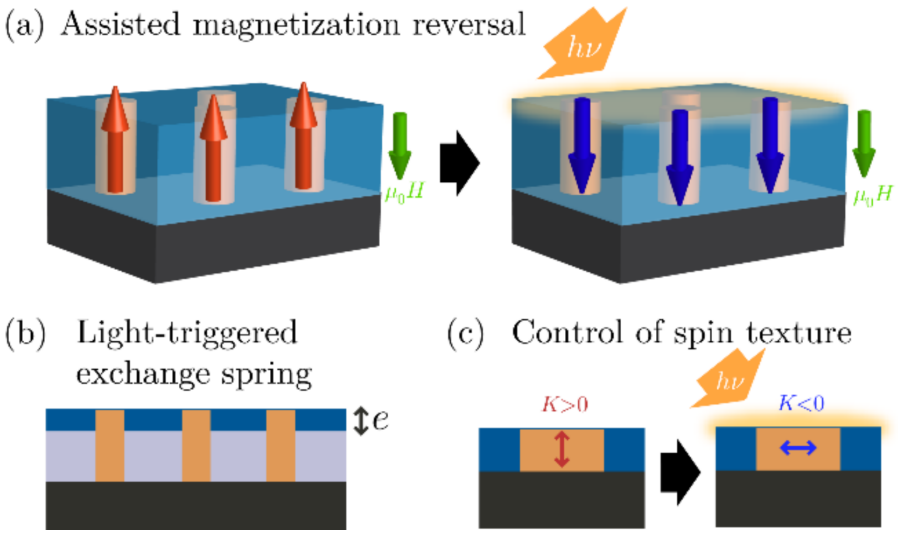

Figure 5.2.: (a) Principle of light-assisted magnetization reversal in ferromagnetic PS VANs in a non-local bias field. (b) Optimized structure with a thin layer of PS material (thickness e) leading to a light-triggered exchange spring system. The soft part corresponds to the apex of the nanopillar in the region of thickness e where its softness is triggered by light. (c) Reconfigurable magnetization textures in optimized nanocomposites: by adjusting static strain and dimensions, we aim at elaborating nanostructures with magnetization switching from out-of-plane to in-plane upon irradiation.

hybrid VANs that couple magnetism and photostriction in order to control the magnetization locally allowing for light-reconfigurable spin textures on an ultrafast timescale. Despite a previous report suggesting that PS-ferromagnetic VANs are interesting systems for control of ferromagnetism through light [122], the field of PS-ferromagnetic VANs has been barely explored since and many questions remain open concerning the optimization of coupling effects in VANs and the timescales and associated speed of action of light on magnetism.

Together with the team of Franck Vidal at Institut des nanosciences de Paris, Guillaume Lambert at LOA and Nicolas Jaouen at Synchrotron Soleil, we have received an ANR grant (starting 1st January 2022) to study ultrafast magnetization dynamics in PS-ferromagnetic VANs.

Glossary

AOS all-optical switching. 4

APD avalanche photodiode. 32–34

FERMI Free Electron Laser Radiation for Multidisciplinary Investigations. 9, 29, 36

FLASH Free electrons LASer in Hamburg. 9, 23, 28, 30, 32, 36

FWHM full width at half maximum. 17, 32, 34

HHG high harmonics generation. 5–7, 15–17, 36

IR infrared. 5, 8, 13, 15, 18–20, 27–30, 32, 36, 37

LCLS Linac Coherent Light Source. 10, 19

LCPMR laboratoire de chimie physique – matière et rayonnement – Paris, France –. 6, 14, 35

LOA laboratoire d'optique appliquée – Palaiseau, France –. 6, 15, 16, 36, 38

MOKE magneto-optical Kerr effect. 4, 12–15, 35

PLD pulsed laser deposition. 37

PMA perpendicular magnetic anisotropy. 23, 25, 35

PS photostrictive. 37, 38

SASE self-amplified spontaneous emission. 9, 10, 26

TMOKE transverse magneto-optical Kerr effect. 13, 14, 28–30

VANs vertically assembled nanocomposites. 37, 38

XFEL X-ray or XUV free electrons laser. 5–7, 9, 10, 19, 23, 26–30, 32, 36

XMCD X-ray magnetic circular dichroism. 10, 11, 15, 16, 28–30, 32, 36

XRMS X-ray resonant magnetic scattering. 6, 15, 17, 19–24

XUV extreme ultraviolet. 5–7, 9, 12–14, 26–35

Bibliography

[1] B. Koopmans, G. Malinowski, F. Dalla Longa, D. Steiauf, M. Fahnle, T. Roth, M. Cinchetti, and M. Aeschlimann, "Explaining the paradoxical diversity of ultrafast laser-induced demagnetization," *Nature Materials*, vol. 9, pp. 259–265, 03 2010.

[2] E. Beaurepaire, J.-C. Merle, A. Daunois, and J.-Y. Bigot, "Ultrafast Spin Dynamics in Ferromagnetic Nickel," *Physical Review Letters*, vol. 76, pp. 4250–4253, May 1996.

[3] A. Vaterlaus, T. Beutler, and F. Meier, "Spin-lattice relaxation time of ferromagnetic gadolinium determined with time-resolved spin-polarized photoemission," *Physical Review Letters*, vol. 67, pp. 3314–3317, Dec 1991.

[4] H.-S. Rhie, H. A. Dürr, and W. Eberhardt, "Femtosecond electron and spin dynamics in Ni/W(110) films," *Physical Review Letters*, vol. 90, p. 247201, Jun 2003.

[5] K. H. Bennemann, "Ultrafast dynamics in solids," *Journal of Physics: Condensed Matter*, vol. 16, pp. R995–R1056, jul 2004.

[6] I. Radu, C. Stamm, N. Pontius, T. Kachel, P. Ramm, J.-U. Thiele, H. A. Dürr, and C. H. Back, "Laser-induced generation and quenching of magnetization on ferh studied with time-resolved x-ray magnetic circular dichroism," *Physical Review B*, vol. 81, p. 104415, Mar 2010.

[7] G. Zhang, Y. Bai, T. Jenkins, and T. F. George, "Laser-induced ultrafast transport and demagnetization at the earliest time: First-principles and real-time investigation," *Journal of Physics: Condensed Matter*, vol. 30, p. 465801, Oct 2018.

[8] W. Töws and G. M. Pastor, "Tuning the laser-induced ultrafast demagnetization of transition metals," *Physical Review B*, vol. 100, p. 024402, Jul 2019.

[9] C. Dornes, Y. Acremann, M. Savoini, M. Kubli, M. J. Neugebauer, E. Abreu, L. Huber, G. Lantz, C. A. Vaz, H. Lemke, *et al.*, "The ultrafast einstein–de haas effect," *Nature*, vol. 565, pp. 209–212, Jan 2019.

[10] M. Hennecke, I. Radu, R. Abrudan, T. Kachel, K. Holldack, R. Mitzner, A. Tsukamoto, and S. Eisebitt, "Angular momentum flow during ultrafast demagnetization of a ferrimagnet," *Physical Review Letters*, vol. 122, p. 157202, Apr 2019.

[11] F. Siegrist, J. A. Gessner, M. Ossiander, C. Denker, Y.-P. Chang, M. C. Schröder, A. Guggenmos, Y. Cui, J. Walowski, U. Martens, *et al.*, "Light-wave dynamic control of magnetism," *Nature*, vol. 571, pp. 240–244, Jun 2019.

[12] M. Battiato, K. Carva, and P. M. Oppeneer, "Superdiffusive Spin Transport as a Mechanism of Ultrafast Demagnetization," *Physical Review Letters*, vol. 105, p. 027203, Jul 2010.

[13] C. D. Stanciu, F. Hansteen, A. V. Kimel, A. Kirilyuk, A. Tsukamoto, A. Itoh, and T. Rasing, "All-Optical Magnetic Recording with Circularly Polarized Light," *Physical Review Letters*, vol. 99, p. 047601, Jul 2007.

[14] K. Vahaplar, A. M. Kalashnikova, A. V. Kimel, D. Hinzke, U. Nowak, R. Chantrell, A. Tsukamoto, A. Itoh, A. Kirilyuk, and T. Rasing, "Ultrafast Path for Optical Magnetization Reversal via a Strongly Nonequilibrium State," *Physical Review Letters*, vol. 103, p. 117201, Sep 2009.

[15] C. H. Back, R. Allenspach, W. Weber, S. S. P. Parkin, D. Weller, E. L. Garwin, and H. C. Siegmann, "Minimum field strength in precessional magnetization reversal," *Science*, vol. 285, no. 5429, pp. 864–867, 1999.

[16] M. Savoini, R. Medapalli, B. Koene, A. R. Khorsand, L. Le Guyader, L. Duò, M. Finazzi, A. Tsukamoto, A. Itoh, F. Nolting, A. Kirilyuk, A. V. Kimel, and T. Rasing, "Highly efficient all-optical switching of magnetization in gdfeco microstructures by interference-enhanced absorption of light," *Physical Review B*, vol. 86, p. 140404, Oct 2012.

[17] B. Vodungbo, J. Gautier, G. Lambert, A. B. Sardinha, M. Lozano, S. Sebban, M. Ducousso, W. Boutu, K. Li, B. Tudu, M. Tortarolo, R. Hawaldar, R. Delaunay, V. López-Flores, J. Arabski, C. Boeglin, H. Merdji, P. Zeitoun, and J. Lüning, "Laser-induced ultrafast demagnetization in the presence of a nanoscale magnetic domain network," *Nature Communications*, vol. 3, p. 999, 08 2012.

[18] I. Radu, K. Vahaplar, C. Stamm, T. Kachel, N. Pontius, H. A. Durr, T. A. Ostler, J. Barker, R. F. L. Evans, R. W. Chantrell, A. Tsukamoto, A. Itoh, A. Kirilyuk, T. Rasing, and A. V. Kimel, "Transient ferromagnetic-like state mediating ultrafast reversal of antiferromagnetically coupled spins," *Nature*, vol. 472, pp. 205–208, 04 2011.

[19] C. Boeglin, E. Beaurepaire, V. Halte, V. Lopez-Flores, C. Stamm, N. Pontius, H. A. Durr, and J.-Y. Bigot, "Distinguishing the ultrafast dynamics of spin and orbital moments in solids," *Nature*, vol. 465, pp. 458–461, 05 2010.

[20] T. Wang, D. Zhu, B. Wu, C. Graves, S. Schaffert, T. Rander, M. Leonard, B. Vodungbo, C. Baumier, D. P. Bernstein, B. Bräuer, V. Cros, S. de Jong, R. Delaunay, A. Fognini, R. Kukreja, S. Lee, V. Lopéz-Flores, J. Mohanty, B. Pfau, H. Popescu, M. Sacchi, A. Barszczak Sardinha, F. Sirotti, P. Zeitoun, M. Messerschmidt, J. J.

Turner, W. F. Schlotter, O. Hellwig, R. Mattana, N. Jaouen, F. Fortuna, Y. Acremann, C. Gutt, H. A. Dürr, E. Beaurepaire, C. Boeglin, S. Eisebitt, G. Grübel, J. Lüning, J. Stöhr, and A. Scherz, "Femtosecond Single-Shot Imaging of Nanoscale Ferromagnetic Order in CoPd Multilayers Using Resonant X-Ray Holography," *Physical Review Letters*, vol. 108, no. 26, p. 267403, 2012.

[21] C. von Korff Schmising, B. Pfau, M. Schneider, C. Günther, M. Giovannella, J. Perron, B. Vodungbo, L. Müller, F. Capotondi, E. Pedersoli, *et al.*, "Imaging Ultrafast Demagnetization Dynamics after a Spatially Localized Optical Excitation," *Physical Review Letters*, vol. 112, no. 21, p. 217203, 2014.

[22] F. Willems, C. v. K. Schmising, D. Weder, C. M. Günther, M. Schneider, B. Pfau, S. Meise, E. Guehrs, J. Geilhufe, A. E. D. Merhe, E. Jal, B. Vodungbo, J. Lüning, B. Mahieu, F. Capotondi, E. Pedersoli, D. Gauthier, M. Manfredda, and S. Eisebitt, "Multi-color imaging of magnetic Co/Pt heterostructures," *Structural Dynamics*, vol. 4, no. 1, p. 014301, 2017.

[23] B. Vodungbo, A. Barszczak Sardinha, J. Gautier, G. Lambert, C. Valentin, M. Lozano, G. Iaquaniello, F. Delmotte, S. Sebban, J. Lüning, and P. Zeitoun, "Polarization control of high order harmonics in the EUV photon energy range," *Optics Express*, vol. 19, pp. 4346–4356, Feb 2011.

[24] G. Lambert, B. Vodungbo, J. Gautier, B. Mahieu, V. Malka, S. Sebban, P. Zeitoun, J. Luning, J. Perron, A. Andreev, S. Stremoukhov, F. Ardana-Lamas, A. Dax, C. P. Hauri, A. Sardinha, and M. Fajardo, "Towards enabling femtosecond helicity-dependent spectroscopy with high-harmonic sources," *Nature Communications*, vol. 6, p. 6167, Feb 2015.

[25] P. A. Franken, A. E. Hill, C. W. Peters, and G. Weinreich, "Generation of optical harmonics," *Physical Review Letters*, vol. 7, pp. 118–119, Aug 1961.

[26] A. McPherson, G. Gibson, H. Jara, U. Johann, T. S. Luk, I. A. McIntyre, K. Boyer, and C. K. Rhodes, "Studies of multiphoton production of vacuum-ultraviolet radiation in the rare gases," *Journal of the Optical Society of America B*, vol. 4, pp. 595–601, Apr 1987.

[27] P. B. Corkum, "Plasma perspective on strong field multiphoton ionization," *Physical Review Letters*, vol. 71, pp. 1994–1997, Sep 1993.

[28] M. Lewenstein, P. Balcou, M. Y. Ivanov, A. L'Huillier, and P. B. Corkum, "Theory of high-harmonic generation by low-frequency laser fields," *Phys. Rev. A*, vol. 49, pp. 2117–2132, Mar 1994.

[29] J. J. Macklin, J. D. Kmetec, and C. L. Gordon, "High-order harmonic generation using intense femtosecond pulses," *Physical Review Letters*, vol. 70, pp. 766–769, Feb 1993.

[30] C. Spielmann, N. H. Burnett, S. Sartania, R. Koppitsch, M. Schnürer, C. Kan, M. Lenzner, P. Wobrauschek, and F. Krausz, "Generation of coherent x-rays in the water window using 5-femtosecond laser pulses," *Science*, vol. 278, no. 5338, pp. 661–664, 1997.

[31] M. Hentschel, R. Kienberger, C. Spielmann, G. A. Reider, N. Milosevic, T. Brabec, P. Corkum, U. Heinzmann, M. Drescher, and F. Krausz, "Attosecond metrology," *Nature*, vol. 414, pp. 509–513, Nov 2001.

[32] P. B. Corkum and F. Krausz, "Attosecond science," *Nature Physics*, vol. 3, pp. 381–387, Jun 2007.

[33] C. G. Durfee, A. R. Rundquist, S. Backus, C. Herne, M. M. Murnane, and H. C. Kapteyn, "Phase matching of high-order harmonics in hollow waveguides," *Physical Review Letters*, vol. 83, pp. 2187–2190, Sep 1999.

[34] S. Kazamias, D. Douillet, F. Weihe, C. Valentin, A. Rousse, S. Sebban, G. Grillon, F. Augé, D. Hulin, and P. Balcou, "Global optimization of high harmonic generation," *Physical Review Letters*, vol. 90, p. 193901, May 2003.

[35] H. Niikura, F. Légaré, R. Hasbani, M. Y. Ivanov, D. M. Villeneuve, and P. B. Corkum, "Probing molecular dynamics with attosecond resolution using correlated wave packet pairs," *Nature*, vol. 421, pp. 826–829, Feb 2003.

[36] F. Lépine, M. Y. Ivanov, and M. J. J. Vrakking, "Attosecond molecular dynamics: fact or fiction?," *Nature Photonics*, vol. 8, pp. 195–204, Mar 2014.

[37] C. La-O-Vorakiat, M. Siemens, M. M. Murnane, H. C. Kapteyn, S. Mathias, M. Aeschlimann, P. Grychtol, R. Adam, C. M. Schneider, J. M. Shaw, H. Nembach, and T. J. Silva, "Ultrafast Demagnetization Dynamics at the M Edges of Magnetic Elements Observed Using a Tabletop High-Harmonic Soft X-Ray Source," *Physical Review Letters*, vol. 103, p. 257402, Dec 2009.

[38] F. Willems, C. T. Smeenk, N. Zhavoronkov, O. Kornilov, I. Radu, M. Schmidbauer, M. Hanke, C. Von Korff Schmising, M. J. Vrakking, and S. Eisebitt, "Probing ultrafast spin dynamics with high-harmonic magnetic circular dichroism spectroscopy," *Physical Review B*, vol. 92, no. 22, pp. 1–5, 2015.

[39] O. Kfir, P. Grychtol, E. Turgut, R. Knut, D. Zusin, D. Popmintchev, T. Popmintchev, H. Nembach, J. M. Shaw, A. Fleischer, H. Kapteyn, M. Murnane, and O. Cohen, "Generation of bright phase-matched circularly-polarized extreme ultraviolet high harmonics," *Nature Photonics*, vol. 9, p. 99, Dec 2014.

[40] J. Feldhaus, J. Arthur, and J. B. Hastings, "X-ray free-electron lasers," *Journal of Physics B: Atomic, Molecular and Optical Physics*, vol. 38, pp. S799–S819, apr 2005.

[41] G. Lambert, T. Hara, D. Garzella, T. Tanikawa, M. Labat, B. Carre, H. Kitamura, T. Shintake, M. Bougeard, S. Inoue, Y. Tanaka, P. Salieres, H. Merdji, O. Chubar, O. Gobert, K. Tahara, and M.-E. Couprie, "Injection of harmonics generated in gas in a free-electron laser providing intense and coherent extreme-ultraviolet light," *Nature physics*, vol. 4, pp. 296–300, Apr 2008.

[42] J. Rossbach, J. R. Schneider, and W. Wurth, "10 years of pioneering x-ray science at the free-electron laser flash at desy," *Physics Reports*, vol. 808, pp. 1–74, 2019. 10 years of pioneering X-ray science at the Free-Electron Laser FLASH at DESY.

[43] E. Allaria, C. Callegari, D. Cocco, W. Fawley, M. Kiskinova, C. Masciovecchio, and F. Parmigiani, "The FERMI@elettra free-electron-laser source for coherent x-ray physics: photon properties, beam transport system and applications," *New Journal of Physics*, vol. 12, p. 075002, jul 2010.

[44] E. Ferrari, C. Spezzani, F. Fortuna, R. Delaunay, F. Vidal, I. Nikolov, P. Cinquegrana, B. Diviacco, D. Gauthier, G. Penco, P. R. Ribič, E. Roussel, M. Trovò, J.-B. Moussy, T. Pincelli, L. Lounis, M. Manfredda, E. Pedersoli, F. Capotondi, C. Svetina, N. Mahne, M. Zangrando, L. Raimondi, A. Demidovich, L. Giannessi, G. De Ninno, M. B. Danailov, E. Allaria, and M. Sacchi, "Widely tunable two-colour seeded free-electron laser source for resonant-pump resonant-probe magnetic scattering," *Nature Communications*, vol. 7, p. 10343, Jan 2016.

[45] B. Rösner, B. Vodungbo, V. Chardonnet, F. Döring, V. A. Guzenko, M. Hennes, A. Kleibert, M. Lebugle, J. Lüning, N. Mahne, A. Merhe, D. Naumenko, I. P. Nikolov, I. Lopez-Quintas, E. Pedersoli, P. R. Ribič, T. Savchenko, B. Watts, M. Zangrando, F. Capotondi, C. David, and E. Jal, "Simultaneous two-color snapshot view on ultrafast charge and spin dynamics in a Fe-Cu-Ni tri-layer," *Structural Dynamics*, vol. 7, no. 5, p. 054302, 2020.

[46] J. M. Glownia, J. Cryan, J. Andreasson, A. Belkacem, N. Berrah, C. I. Blaga, C. Bostedt, J. Bozek, L. F. DiMauro, L. Fang, J. Frisch, O. Gessner, M. Gühr, J. Hajdu, M. P. Hertlein, M. Hoener, G. Huang, O. Kornilov, J. P. Marangos, A. M. March, B. K. McFarland, H. Merdji, V. S. Petrovic, C. Raman, D. Ray, D. A. Reis, M. Trigo, J. L. White, W. White, R. Wilcox, L. Young, R. N. Coffee, and P. H. Bucksbaum, "Time-resolved pump-probe experiments at the lcls," *Opt. Express*, vol. 18, pp. 17620–17630, Aug 2010.

[47] A. A. Lutman, J. P. MacArthur, M. Ilchen, A. O. Lindahl, J. Buck, R. N. Coffee, G. L. Dakovski, L. Dammann, Y. Ding, H. A. Dürr, L. Glaser, J. Grünert, G. Hartmann, N. Hartmann, D. Higley, K. Hirsch, Y. I. Levashov, A. Marinelli, T. Maxwell, A. Mitra, S. Moeller, T. Osipov, F. Peters, M. Planas, I. Shevchuk, W. F. Schlotter, F. Scholz, J. Seltmann, J. Viefhaus, P. Walter, Z. R. Wolf, Z. Huang, and H.-D. Nuhn, "Polarization control in an x-ray free-electron laser," *Nature Photonics*, vol. 10, pp. 468–472, Jul 2016.

[48] A. e. d. Merhe, *Ultrafast modification of the magnetic anisotropy in a CoTb alloy.* PhD thesis, Sorbonne Université, 2018.

[49] B. T. Thole, G. van der Laan, and G. A. Sawatzky, "Strong magnetic dichroism predicted in the $M_{4,5}$ x-ray absorption spectra of magnetic rare-earth materials," *Physical Review Letters*, vol. 55, pp. 2086–2088, Nov 1985.

[50] G. Schütz, R. Frahm, P. Mautner, R. Wienke, W. Wagner, W. Wilhelm, and P. Kienle, "Spin-dependent extended x-ray-absorption fine structure: Probing magnetic short-range order," *Physical Review Letters*, vol. 62, pp. 2620–2623, May 1989.

[51] G. Schütz, M. Knülle, R. Wienke, W. Wilhelm, W. Wagner, P. Kienle, and R. Frahm, "Spin-dependent photoabsorption at the l-edges of ferromagnetic gd and tb metal," *Zeitschrift für Physik B Condensed Matter*, vol. 73, pp. 67–75, Mar 1988.

[52] G. van der Laan, B. T. Thole, G. A. Sawatzky, J. B. Goedkoop, J. C. Fuggle, J.-M. Esteva, R. Karnatak, J. P. Remeika, and H. A. Dabkowska, "Experimental proof of magnetic x-ray dichroism," *Physical Review B*, vol. 34, pp. 6529–6531, Nov 1986.

[53] P. Rudolf, F. Sette, L. Tjeng, G. Meigs, and C. Chen, "Magnetic moments in a gadolinium iron garnet studied by soft-x-ray magnetic circular dichroism," *Journal of Magnetism and Magnetic Materials*, vol. 109, no. 1, pp. 109–112, 1992.

[54] C. T. Chen, F. Sette, Y. Ma, and S. Modesti, "Soft-x-ray magnetic circular dichroism at the $L_{2,3}$ edges of nickel," *Physical Review B*, vol. 42, pp. 7262–7265, Oct 1990.

[55] T. Koide, T. Shidara, H. Fukutani, K. Yamaguchi, A. Fujimori, and S. Kimura, "Strong magnetic circular dichroism at the $M_{2,3}$ edges in ferromagnetic Ni and ferrimagnetic Fe_3O_4," *Physical Review B*, vol. 44, pp. 4697–4700, Sep 1991.

[56] H. Höchst, D. Zhao, and D. L. Huber, "$M_{2,3}$ magnetic circular dichroism (MCD) measurements of Fe, Co and Ni using a newly developed quadruple reflection phase shifter," *Surface Science*, vol. 352–354, pp. 998–1002, May 1996. Proceedings of the 15th European Conference on Surface Science.

[57] J. Stöhr and H. C. Siegmann, "Magnetism," *Solid-State Sciences. Springer, Berlin, Heidelberg*, vol. 5, 2006.

[58] C. Alves, *Studying ultrafast magnetization dynamics through Faraday effect and using linearly polarized high order harmonics.* PhD thesis, Sorbonne Université, 2018.

[59] M. Faraday, "On the magnetization of light and the illumination of magnetic lines of force," *Philosophical Transactions of the Royal Society of London*, vol. 136, pp. 1–20, 1846.

[60] H.-C. Mertins, F. Schäfers, X. Le Cann, A. Gaupp, and W. Gudat, "Faraday rotation at the 2p edges of fe, co, and ni," *Physical Review B*, vol. 61, pp. R874–R877, Jan 2000.

[61] S. Valencia, A. Gaupp, W. Gudat, H. Mertins, *et al.*, "Faraday rotation spectra at shallow core levels: 3*p* edges of Fe, Co, and Ni," *New Journal of Physics*, vol. 8, p. 254, 2006.

[62] J. Kuneš, P. Oppeneer, H.-C. Mertins, F. Schäfers, A. Gaupp, W. Gudat, and P. Novák, "X-ray Faraday effect at the L 2, 3 edges of Fe, Co, and Ni: theory and experiment," *Physical Review B*, vol. 64, no. 17, p. 174417, 2001.

[63] C. Alves, G. Lambert, V. Malka, M. Hehn, G. Malinowski, M. Hennes, V. Chardonnet, E. Jal, J. Lüning, and B. Vodungbo, "Resonant faraday effect using high-order harmonics for the investigation of ultrafast demagnetization," *Physical Review B*, vol. 100, no. 14, p. 144421, 2019.

[64] X. Liu, *Investigation of the early time period of ultrafast magnetization dynamics*. PhD thesis, Sorbonne Université, 2018.

[65] John Kerr LL.D., "XLIII. On rotation of the plane of polarization by reflection from the pole of a magnet," *The London, Edinburgh, and Dublin Philosophical Magazine and Journal of Science*, vol. 3, no. 19, pp. 321–343, 1877.

[66] S. Bader, "Smoke," *JMMM*, vol. 100, no. 1, pp. 440–454, 1991.

[67] H. Höchst, D. Rioux, D. Zhao, and D. L. Huber, "Magnetic linear dichroism effects in reflection spectroscopy: A case study at the Fe $M_{2,3}$ edge," *Journal of Applied Physics*, vol. 81, pp. 7584–7588, Jun 1997.

[68] C. La-O-Vorakiat, E. Turgut, C. A. Teale, H. C. Kapteyn, M. M. Murnane, S. Mathias, M. Aeschlimann, C. M. Schneider, J. M. Shaw, H. T. Nembach, and T. J. Silva, "Ultrafast Demagnetization Measurements Using Extreme Ultraviolet Light: Comparison of Electronic and Magnetic Contributions," *Physical Review X*, vol. 2, p. 011005, Jan 2012.

[69] B. Vodungbo, J. Gautier, G. Lambert, P. Zeitoun, and J. Lüning, "Comment on"Ultrafast Demagnetization Measurements Using Extreme Ultraviolet Light: Comparison of Electronic and Magnetic Contributions"," *Physical Review X*, vol. 3, no. 3, p. 38001, 2013.

[70] P. Kelly and R. Arnell, "Magnetron sputtering: a review of recent developments and applications," *Vacuum*, vol. 56, no. 3, pp. 159–172, 2000.

[71] O. Hellwig, G. Denbeaux, J. Kortright, and E. E. Fullerton, "X-ray studies of aligned magnetic stripe domains in perpendicular multilayers," *Physica B: Condensed Matter*, vol. 336, no. 1-2, pp. 136–144, 2003.

[72] C. Gutt, L. Stadler, S. Streit-Nierobisch, A. Mancuso, A. Schropp, B. Pfau, C. Günther, R. Könnecke, J. Gulden, B. Reime, *et al.*, "Resonant magnetic scattering with soft x-ray pulses from a free-electron laser operating at 1.59 nm," *Physical Review B*, vol. 79, no. 21, p. 212406, 2009.

[73] C. Gutt, S. Streit-Nierobisch, L. Stadler, B. Pfau, C. Günther, R. Könnecke, R. Frömter, A. Kobs, D. Stickler, H. Oepen, *et al.*, "Single-pulse resonant magnetic scattering using a soft x-ray free-electron laser," *Physical Review B*, vol. 81, no. 10, p. 100401, 2010.

[74] J. W. Goodman, *Introduction to Fourier optics*. Englewood: Roberts & Company Publishers, 2005.

[75] J. B. Kortright and S.-K. Kim, "Resonant magneto-optical properties of Fe near its $2p$ levels: Measurement and applications," *Physical Review B*, vol. 62, pp. 12216–12228, Nov 2000.

[76] Y. Mairesse, O. Gobert, P. Breger, H. Merdji, P. Meynadier, P. Monchicourt, M. Perdrix, P. Salières, and B. Carré, "High Harmonic XUV Spectral Phase Interferometry for Direct Electric-Field Reconstruction," *Physical Review Letters*, vol. 94, p. 173903, May 2005.

[77] E. Papalazarou, D. Boschetto, J. Gautier, T. Garl, C. Valentin, G. Rey, P. Zeitoun, A. Rousse, P. Balcou, and M. Marsi, "Probing coherently excited optical phonons by extreme ultraviolet radiation with femtosecond time resolution," *Applied Physics Letters*, vol. 93, p. 041114, 2008.

[78] G. Malinowski, F. Dalla Longa, J. H. H. Rietjens, P. V. Paluskar, R. Huijink, H. J. M. Swagten, and B. Koopmans, "Control of speed and efficiency of ultrafast demagnetization by direct transfer of spin angular momentum," *Nature Physics*, vol. 4, pp. 855–858, 11 2008.

[79] M. Battiato, K. Carva, and P. M. Oppeneer, "Theory of laser-induced ultrafast superdiffusive spin transport in layered heterostructures," *Physical Review B*, vol. 86, p. 024404, Jul 2012.

[80] B. Pfau, S. Schaffert, L. Müller, C. Gutt, A. Al-Shemmary, F. Büttner, R. Delaunay, S. Düsterer, S. Flewett, R. Frömter, J. Geilhufe, E. Guehrs, C. M. Günther, R. Hawaldar, M. Hille, N. Jaouen, A. Kobs, K. Li, J. Mohanty, H. Redlin, W. F. Schlotter, D. Stickler, R. Treusch, B. Vodungbo, M. Kläui, H. P. Oepen, J. Lüning, G. Grübel, and S. Eisebitt, "Ultrafast optical demagnetization manipulates nanoscale spin structure in domain walls," *Nature Communications*, vol. 3, p. 1100, 10 2012.

[81] D. Rudolf, C. La-O-Vorakiat, M. Battiato, R. Adam, J. M. Shaw, E. Turgut, P. Maldonado, S. Mathias, P. Grychtol, H. T. Nembach, T. J. Silva, M. Aeschlimann, H. C. Kapteyn, M. M. Murnane, C. M. Schneider, and P. M. Oppeneer, "Ultrafast magnetization enhancement in metallic multilayers driven by superdiffusive spin current," *Nature Communications*, vol. 3, p. 1037, 09 2012.

[82] T. Kampfrath, M. Battiato, P. Maldonado, G. Eilers, J. Nötzold, S. Mährlein, V. Zbarsky, F. Freimuth, Y. Mokrousov, S. Blügel, M. Wolf, I. Radu, P. M. Oppeneer, and M. Münzenberg, "Terahertz spin current pulses controlled by magnetic heterostructures," *Nature Nanotechnology*, vol. 8, pp. 256–260, Apr. 2013.

[83] A. Eschenlohr, M. Battiato, P. Maldonado, N. Pontius, T. Kachel, K. Holldack, R. Mitzner, A. Föhlisch, P. M. Oppeneer, and C. Stamm, "Ultrafast spin transport as key to femtosecond demagnetization," *Nature Materials*, vol. 12, pp. 332–336, Apr. 2013.

[84] B. Vodungbo, B. Tudu, J. Perron, R. Delaunay, L. Müller, M. H. Berntsen, G. Grübel, G. Malinowski, C. Weier, J. Gautier, *et al.*, "Indirect excitation of ultrafast demagnetization," *Scientific Report*, vol. 6, p. 18970, 2016.

[85] I. P. Batra and L. Kleinman, "Chemisorption of oxygen on aluminum surfaces," *Journal of Electron Spectroscopy and Related Phenomena*, vol. 33, no. 3, pp. 175–241, 1984.

[86] W. F. Schlotter, J. J. Turner, M. Rowen, P. Heimann, M. Holmes, O. Krupin, M. Messerschmidt, S. Moeller, J. Krzywinski, R. Soufli, M. Fernández-Perea, N. Kelez, S. Lee, R. Coffee, G. Hays, M. Beye, N. Gerken, F. Sorgenfrei, S. Hau-Riege, L. Juha, J. Chalupsky, V. Hajkova, A. P. Mancuso, A. Singer, O. Yefanov, I. A. Vartanyants, G. Cadenazzi, B. Abbey, K. A. Nugent, H. Sinn, J. Lüning, S. Schaffert, S. Eisebitt, W.-S. Lee, A. Scherz, A. R. Nilsson, and W. Wurth, "The soft x-ray instrument for materials studies at the linac coherent light source x-ray free-electron laser," *Review of Scientific Instruments*, vol. 83, no. 4, p. 043107, 2012.

[87] L. Strüder, S. Epp, D. Rolles, R. Hartmann, P. Holl, G. Lutz, H. Soltau, R. Eckart, C. Reich, K. Heinzinger, C. Thamm, A. Rudenko, F. Krasniqi, K.-U. Kühnel, C. Bauer, C.-D. Schröter, R. Moshammer, S. Techert, D. Miessner, M. Porro, O. Hälker, N. Meidinger, N. Kimmel, R. Andritschke, F. Schopper, G. Weidenspointner, A. Ziegler, D. Pietschner, S. Herrmann, U. Pietsch, A. Walenta, W. Leitenberger, C. Bostedt, T. Möller, D. Rupp, M. Adolph, H. Graafsma, H. Hirsemann, K. Gärtner, R. Richter, L. Foucar, R. L. Shoeman, I. Schlichting, and J. Ullrich, "Large-format, high-speed, X-ray pnCCDs combined with electron and ion imaging spectrometers in a multipurpose chamber for experiments at 4th generation light sources," *Nuclear Instruments and Methods in Physics Research Section A: Accelerators, Spectrometers, Detectors and Associated Equipment*, vol. 614, no. 3, pp. 483–496, 2010.

[88] G. L. Dakovski, P. Heimann, M. Holmes, O. Krupin, M. P. Minitti, A. Mitra, S. Moeller, M. Rowen, W. F. Schlotter, and J. J. Turner, "The Soft X-ray Research instrument at the Linac Coherent Light Source," *Journal of Synchrotron Radiation*, vol. 22, pp. 498–502, May 2015.

[89] M. Beye, O. Krupin, G. Hays, A. H. Reid, D. Rupp, S. d. Jong, S. Lee, W.-S. Lee, Y.-D. Chuang, R. Coffee, J. P. Cryan, J. M. Glownia, A. Föhlisch, M. R. Holmes, A. R. Fry, W. E. White, C. Bostedt, A. O. Scherz, H. A. Durr, and W. F. Schlotter, "X-ray pulse preserving single-shot optical cross-correlation method for improved experimental temporal resolution," *Applied Physics Letters*, vol. 100, no. 12, p. 121108, 2012.

[90] Moisan N., Malinowski G., Mauchain J., Hehn M., Vodungbo B., Luning J., Mangin S., Fullerton E. E., and Thiaville A., "Investigating the role of superdiffusive currents in laser induced demagnetization of ferromagnets with nanoscale magnetic domains," *Scientific Report*, vol. 4, p. 4658, apr 2014.

[91] D. Zusin, E. Iacocca, L. L. Guyader, A. H. Reid, W. F. Schlotter, T.-M. Liu, D. J. Higley, G. Coslovich, S. F. Wandel, P. M. Tengdin, S. K. K. Patel, A. Shabalin, N. Hua, S. B. Hrkac, H. T. Nembach, J. M. Shaw, S. A. Montoya, A. Blonsky, C. Gentry, M. A. Hoefer, M. M. Murnane, H. C. Kapteyn, E. E. Fullerton, O. Shpyrko, H. A. Dürr, and T. J. Silva, "Ultrafast domain dilation induced by optical pumping in ferromagnetic cofe/ni multilayers," 2020.

[92] M. Hennes, A. Merhe, X. Liu, D. Weder, C. v. K. Schmising, M. Schneider, C. M. Günther, B. Mahieu, G. Malinowski, M. Hehn, D. Lacour, F. Capotondi, E. Pedersoli, I. P. Nikolov, V. Chardonnet, E. Jal, J. Lüning, and B. Vodungbo, "Laser-induced ultrafast demagnetization and perpendicular magnetic anisotropy reduction in a $co_{88}tb_{12}$ thin film with stripe domains," *Physical Review B*, vol. 102, p. 174437, Nov 2020.

[93] J. T. Fourkas, L. Dhar, K. A. Nelson, and R. Trebino, "Spatially encoded, single-shot ultrafast spectroscopies," *J. Opt. Soc. Am. B*, vol. 12, pp. 155–165, Jan 1995.

[94] P. R. Poulin and K. A. Nelson, "Irreversible organic crystalline chemistry monitored in real time," *Science*, vol. 313, no. 5794, pp. 1756–1760, 2006.

[95] K. Nakagawa, A. Iwasaki, Y. Oishi, R. Horisaki, A. Tsukamoto, A. Nakamura, K. Hirosawa, H. Liao, T. Ushida, K. Goda, F. Kannari, and I. Sakuma, "Sequentially timed all-optical mapping photography (stamp)," *Nature Photonics*, vol. 8, pp. 695–700, Sep 2014.

[96] David C., Karvinen P., Sikorski M., Song S., Vartiainen I., Milne C. J., Mozzanica A., Kayser Y., Diaz A., Mohacsi I., Carini G. A., Herrmann S., Färm E., Ritala M., Fritz D. M., and Robert A., "Following the dynamics of matter with femtosecond precision using the X-ray streaking method," *Scientific Reports*, vol. 5, p. 7644, jan 2015.

[97] M. Buzzi, M. Makita, L. Howald, A. Kleibert, B. Vodungbo, P. Maldonado, J. Raabe, N. Jaouen, H. Redlin, K. Tiedtke, *et al.*, "Single-shot Monitoring of Ultrafast Processes via X-ray Streaking at a Free Electron Laser," *Scientific Report*, vol. 7, p. 7253, 2017.

[98] P. Karvinen, S. Rutishauser, A. Mozzanica, D. Greiffenberg, P. N. Juranić, A. Menzel, A. Lutman, J. Krzywinski, D. M. Fritz, H. T. Lemke, M. Cammarata, and C. David, "Single-shot analysis of hard x-ray laser radiation using a noninvasive grating spectrometer," *Opt. Lett.*, vol. 37, pp. 5073–5075, Dec 2012.

[99] P. Emma, R. Akre, J. Arthur, R. Bionta, C. Bostedt, J. Bozek, A. Brachmann, P. Bucksbaum, R. Coffee, F. J. Decker, Y. Ding, D. Dowell, S. Edstrom, A. Fisher, FrischJ., GilevichS., HastingsJ., HaysG., HeringPh., HuangZ., IversonR., LoosH., MesserschmidtM., MiahnahriA., MoellerS., N. D., PileG., RatnerD., RzepielaJ., SchultzD., SmithT., StefanP., TompkinsH., TurnerJ., WelchJ., WhiteW., WuJ., YockyG., and GalaydaJ., "First lasing and operation of an angstrom-wavelength free-electron laser," *Nature Photonics*, vol. 4, pp. 641–647, 09 2010.

[100] C. Pellegrini, A. Marinelli, and S. Reiche, "The physics of x-ray free-electron lasers," *Rev. Mod. Phys.*, vol. 88, p. 015006, Mar 2016.

[101] E. Jal, M. Makita, B. Rösner, C. David, F. Nolting, J. Raabe, T. Savchenko, A. Kleibert, F. Capotondi, E. Pedersoli, L. Raimondi, M. Manfredda, I. Nikolov, X. Liu, A. e. d. Merhe, N. Jaouen, J. Gorchon, G. Malinowski, M. Hehn, B. Vodungbo, and J. Lüning, "Single-shot time-resolved magnetic x-ray absorption at a free-electron laser," *Physical Review B*, vol. 99, p. 144305, Apr 2019.

[102] W. Helml, I. Grguraš, P. N. Juranić, S. Düsterer, T. Mazza, A. R. Maier, N. Hartmann, M. Ilchen, G. Hartmann, L. Patthey, C. Callegari, J. T. Costello, M. Meyer, R. N. Coffee, A. L. Cavalieri, and R. Kienberger, "Ultrashort free-electron laser x-ray pulses," *Applied Sciences*, vol. 7, no. 9, 2017.

[103] R. Ivanov, J. Liu, G. Brenner, M. Brachmanski, and S. Düsterer, "FLASH free-electron laser single-shot temporal diagnostic: terahertz-field-driven streaking," *Journal of Synchrotron Radiation*, vol. 25, pp. 26–31, Jan 2018.

[104] B. Mahieu, E. Allaria, D. Castronovo, M. B. Danailov, A. Demidovich, G. D. Ninno, S. D. Mitri, W. M. Fawley, E. Ferrari, L. Fröhlich, D. Gauthier, L. Giannessi, N. Mahne, G. Penco, L. Raimondi, S. Spampinati, C. Spezzani, C. Svetina, M. Trovò, and M. Zangrando, "Two-colour generation in a chirped seeded free-electron laser: a close look," *Opt. Express*, vol. 21, pp. 22728–22741, Sep 2013.

[105] A. A. Lutman, T. J. Maxwell, J. P. MacArthur, M. W. Guetg, N. Berrah, R. N. Coffee, Y. Ding, Z. Huang, A. Marinelli, S. Moeller, and J. C. U. Zemella, "Fresh-slice multicolour x-ray free-electron lasers," *Nature Photonics*, vol. 10, pp. 745–750, Nov 2016.

[106] X. Liu, A. Merhe, E. Jal, R. Delaunay, R. Jarrier, V. Chardonnet, M. Hennes, S. G. Chiuzbaian, K. Légaré, M. Hennecke, I. Radu, C. V. K. Schmising, S. Grunewald, M. Kuhlmann, J. Lüning, and B. Vodungbo, "Sub-15-fs x-ray pump and x-ray probe experiment for the study of ultrafast magnetization dynamics in ferromagnetic alloys," *Optics Express*, vol. 29, pp. 32388–32403, Sep 2021.

[107] M. Hennes, B. Rösner, V. Chardonnet, G. S. Chiuzbaian, R. Delaunay, F. Döring, V. A. Guzenko, M. Hehn, R. Jarrier, A. Kleibert, M. Lebugle, J. Lüning, G. Malinowski, A. Merhe, D. Naumenko, I. P. Nikolov, I. Lopez-Quintas, E. Pedersoli, T. Savchenko, B. Watts, M. Zangrando, C. David, F. Capotondi, B. Vodungbo, and E. Jal, "Time-resolved xuv absorption spectroscopy and magnetic circular dichroism at the ni m2,3-edges," *Applied Sciences*, vol. 11, no. 1, 2021.

[108] C. Stamm, T. Kachel, N. Pontius, R. Mitzner, T. Quast, K. Holldack, S. Khan, C. Lupulescu, E. F. Aziz, M. Wietstruk, H. A. Durr, and W. Eberhardt, "Femtosecond modification of electron localization and transfer of angular momentum in nickel," *Nature Materials*, vol. 6, pp. 740–743, 10 2007.

[109] T. Kachel, N. Pontius, C. Stamm, M. Wietstruk, E. F. Aziz, H. A. Dürr, W. Eberhardt, and F. M. F. de Groot, "Transient electronic and magnetic structures of nickel heated by ultrafast laser pulses," *Physical Review B*, vol. 80, p. 092404, Sep 2009.

[110] K. Carva, D. Legut, and P. M. Oppeneer, "Influence of laser-excited electron distributions on the X-ray magnetic circular dichroism spectra: Implications for femtosecond demagnetization in Ni," *EPL*, vol. 86, no. 5, p. 57002, 2009.

[111] L. Müller, C. Gutt, B. Pfau, S. Schaffert, J. Geilhufe, F. Büttner, J. Mohanty, S. Flewett, R. Treusch, S. Düsterer, *et al.*, "Breakdown of the X-ray resonant magnetic scattering signal during intense pulses of extreme ultraviolet free-electron-laser radiation," *Physical Review Letters*, vol. 110, no. 23, p. 234801, 2013.

[112] J. Stöhr and A. Scherz, "Creation of X-Ray Transparency of Matter by Stimulated Elastic Forward Scattering," *Physical Review Letters*, vol. 115, p. 107402, Sep 2015.

[113] B. Wu, T. Wang, C. Graves, D. Zhu, W. Schlotter, J. Turner, O. Hellwig, Z. Chen, H. Dürr, A. Scherz, *et al.*, "Elimination of x-ray diffraction through stimulated x-ray transmission," *Physical Review Letters*, vol. 117, no. 2, p. 027401, 2016.

[114] M. Schneider, B. Pfau, C. M. Günther, C. von Korff Schmising, D. Weder, J. Geilhufe, J. Perron, F. Capotondi, E. Pedersoli, M. Manfredda, M. Hennecke, B. Vodungbo, J. Lüning, and S. Eisebitt, "Ultrafast demagnetization dominates fluence dependence of magnetic scattering at co m edges," *Physical Review Letters*, vol. 125, p. 127201, Sep 2020.

[115] S. Mangin, D. Ravelosona, J. A. Katine, M. J. Carey, B. D. Terris, and E. E. Fullerton, "Current-induced magnetization reversal in nanopillars with perpendicular anisotropy," *Nature Materials*, vol. 5, pp. 210–215, Mar 2006.

[116] Y.-H. Chu, L. W. Martin, M. B. Holcomb, M. Gajek, S.-J. Han, Q. He, N. Balke, C.-H. Yang, D. Lee, W. Hu, Q. Zhan, P.-L. Yang, A. Fraile-Rodríguez, A. Scholl, S. X. Wang, and R. Ramesh, "Electric-field control of local ferromagnetism using a magnetoelectric multiferroic," *Nature Materials*, vol. 7, pp. 478–482, Jun 2008.

[117] B. Kundys, "Photostrictive materials," *Applied Physics Reviews*, vol. 2, no. 1, p. 011301, 2015.

[118] T.-C. Wei, H.-P. Wang, H.-J. Liu, D.-S. Tsai, J.-J. Ke, C.-L. Wu, Y.-P. Yin, Q. Zhan, G.-R. Lin, Y.-H. Chu, and J.-H. He, "Photostriction of strontium ruthenate," *Nature Communications*, vol. 8, p. 15018, Apr 2017.

[119] J.-C. Yang, Y.-D. Liou, W.-Y. Tzeng, H.-J. Liu, Y.-W. Chang, P.-H. Xiang, Z. Zhang, C.-G. Duan, C.-W. Luo, Y.-C. Chen, and Y.-H. Chu, "Ultrafast Giant Photostriction of Epitaxial Strontium Iridate Film with Superior Endurance," *Nano Letters*, vol. 18, no. 12, pp. 7742–7748, 2018. PMID: 30407834.

[120] F. J. Bonilla, A. Novikova, F. Vidal, Y. Zheng, E. Fonda, D. Demaille, V. Schuler, A. Coati, A. Vlad, Y. Garreau, M. Sauvage Simkin, Y. Dumont, S. Hidki, and V. Etgens, "Combinatorial Growth and Anisotropy Control of Self-Assembled Epitaxial Ultrathin Alloy Nanowires," *ACS Nano*, vol. 7, no. 5, pp. 4022–4029, 2013. PMID: 23627649.

[121] M. Hennes, X. Weng, E. Fonda, B. Gallas, G. Patriarche, D. Demaille, Y. Zheng, and F. Vidal, "Phase separation and surface segregation in $Co - -Au - -srtio_3$ thin films: Self-assembly of bilayered epitaxial nanocolumnar composites," *Phys. Rev. Materials*, vol. 3, p. 035002, Mar 2019.

[122] H.-J. Liu, L.-Y. Chen, Q. He, C.-W. Liang, Y.-Z. Chen, Y.-S. Chien, Y.-H. Hsieh, S.-J. Lin, E. Arenholz, C.-W. Luo, Y.-L. Chueh, Y.-C. Chen, and Y.-H. Chu, "Epitaxial Photostriction–Magnetostriction Coupled Self-Assembled Nanostructures," *ACS Nano*, vol. 6, no. 8, pp. 6952–6959, 2012. PMID: 22746982.

A. Résumé en français

Dans ce rapport, je résume mes activités de recherche des dix dernières années dans le domaine de la dynamique d'aimantation ultrarapide. La spécificité de mon approche est d'utiliser des impulsions de rayons X femtosecondes pour sonder l'aimantation de la matière. Ce type d'études a été rendu possible grâce à la mise au point de source de rayons X femtosecondes comme la génération d'harmoniques d'ordre élevé ou les lasers à électrons libre X. L'utilisation de rayons X pour sonder l'aimantation de la matière présente plusieurs avantages dont : l'obtention d'une résolution spatiale nanométrique pour étudier l'aimantation à l'échelle des plus petites structures magnétiques ; la spécifité élémentaire pour observer la dynamique magnétique de différents éléments dans des alliages ou hétérostructures ; une résolution temporelle pouvant aller jusqu'à l'échelle attoseconde ; la possibilité de séparer les contributions de spin et orbital à l'aimantation.

Les expériences réalisées reposent sur différents effets magnéto-optiques qui permettent de mesurer l'état de l'aimantation d'un système avec de la lumière. Dans ces études nous avons exploité : (i) le dichroisme magnétique circulaire des rayons X (XMCD) ; (ii) l'effet Faraday ; (iii) l'effet Kerr magnéto-optique transverse (TMOKE). L'application de l'effet XMCD à des échantillons présentant des domaines magnétiques nanométriques alignés nous à permis d'étudier pour la première fois la désaimantation ultrarapide à l'échelle nanométrique. En effet, grâce à l'effet XMCD cette structure se comporte comme un réseau de diffraction pour des rayons X en résonance avec des seuils d'absorption des matériaux étudiés. Les pics de diffusion observés sont caractéristiques de la structure magnétique et peuvent être étudiés après stimulation par une impulsion optique femtoseconde qui pousse le système dans un état hors équilibre. Grâce à ce type d'expériences, nous avons pu mettre en évidence la désaimantation induite par électrons chauds, nous avons pu étudier le transport superdiffusif de spin dans des multicouches ou encore nous avons pu suivre la dynamique de l'anisotropie magnétique perpendiculaire.

Nous avons également mis au point des techniques permenttant d'observer de manière plus poussée la dynamique magnétique ultrarapide. Par exemple, nous avons démontré la possibilité d'enregistrer la dynamique magnétique avec une seule impulsion X ce qui ouvre la voie à l'étude de phénomènes irréversibles ou à l'obtention de données avec un excellent rapport signal sur bruit. Par ailleurs, nous avons pu repousser les limites de la résolution temporelle pour des études de physique du solide sur laser à électrons libres dans une configuration expérimentale pompe X sonde X qui ouvre des perspectives pour l'étude d'effets cohérents sub-femtoseconde.

Les perspectives de ce travail sont nombreuses mais dans les prochaines années je souhaite me consacrer à deux projets. Avec le groupe de Franck Vidal de l'institut des nanosciences de Paris nous avons obtenu un financement ANR pour étudier la dynamique d'aimantation dans des nano-pilliers magnétiques intégrés dans des matrices

photostrictives. L'objectif est de controler l'aimantation des pilliers avec des impulsions femtosecondes. Je souhaite également étudier l'influence de la dynamique de la structure électronique sur la dynamique magnétique. En effet, nous avons obtenus plusieurs résultats qui indiquent qu'ils faut tenir compte de l'évolution de la structure électronique pour bien rendre compte de la dynamique d'aimantation.

B. CV

Boris Vodungbo

Maître de conférences

Sorbonne Université

4 place Jussieu
75252 Paris, France
+33 (0)6 81 01 60 43
+33 (0)1 44 27 66 17
boris.vodungbo@sorbonne-universite.fr
31/08/1981

Research interests

- Ultrafast magnetization dynamics of thin films
- Development of novel spectroscopic instrumentations based on femtosecond X-UV sources for the study of ultrafast electronic dynamics

Professionnal experience

Since 09/2013 **Assistant Professor**, *Laboratoire de Chimie Physique – Matière et Rayonnement*, Paris, France.

12/2010–08/2013 **Postdoctoral fellow**, *Laboratoire d'Optique Appliquée*, Palaiseau, France.
Femtosecond X-UV sources applied to the study ultrafast magnetization dynamics

12/2008–11/2009 **Postdoctoral fellow**, *Laboratoire de Chimie Physique – Matière et Rayonnement*, Paris, France.
Organisation dynamics of polymer thin films studied by resonant X-ray reflectivity

09/2004–12/2007 **Ph.D. student**, *Institut des Nanosciences de Paris*, Paris, France.
Magnetic oxides for spintronics applications

Teaching

Undergraduate

2019– **Mathematics**, *30 hours/year*.

2014– **Physics for health sciences**, *50 hours/year*.

2013– **Chemistry**, *80 hours/year*.

Master

2018– **X-ray spectroscopy**, *30 hours/year*.

2014– **Bibliography**, *15 hours/year*.

Supervision

Postdoctoral fellows

2019–2021 **Marcel Hennes**, Director: Boris Vodungbo (50%), Co-director: Emmanuelle Jal (50%).

2015–2017 **Emmanuelle Jal**, Director: Jan Lüning (50%), Co-director: Boris Vodungbo (50%).

PhD students

2018–2022 **Valentin Chardonnet**, *Étude de la désaimantation ultrarapide à l'aide de la réflectivité magnétique résonante*, Director: Gheorghe S. Chiuzbăian (20%), Co-directors: Boris Vodungbo (40%), Emmanuelle Jal (40%).

2015–2018 **Alaa el dine Merhe**, *Ultrafast modification of the magnetic anisotropy in a CoTb alloy*, Director: Jan Lüning (50%), Co-director: Boris Vodungbo (50%).

2015–2018 **Xuan Liu**, *Investigation of the early time period of ultrafast magnetization dynamics*, Director: Jan Lüning (50%), Co-director: Boris Vodungbo (50%).

2015–2018 **Carla Alves**, *Studying ultrafast magnetization dynamics through Faraday effect and using linearly polarized high order harmonics*, Director: Jan Lüning (50%), Co-director: Boris Vodungbo (50%).

2011–2016 **Anna Luiza Barszczak Sardinha**, *Coherent imaging of nano-objects with ultra-short X-ray pulses*, Director: Philippe Zeitoun (50%), Co-director: Boris Vodungbo (50%).

2007–2010 **Ma Wei**, *Caractérisation du processus de réorganisation moléculaire en couche mince de copolymère à bloc et développement de la technique diffusion rayons X mous résonante*, Director: Jan Lüning (50%), Co-director: Boris Vodungbo (50%).

Master students

2021 **Cathy Vang**, *Optimization of Co_xTb_{1-x} alloy thin films with perpendicular anisotropy*, Director: Emmanuelle Jal (50%), Co-director: Boris Vodungbo (50%).

2018 **Katherine Légaré**, *Optimization of MOKE setups for magnetic thin film characterization*, Director: Boris Vodungbo (50%), Co-director: Emmanuelle Jal (50%).

2018 **Heba Hamdam**, *Realization of magnetic thin films by magnetron sputtering*, Director: Emmanuelle Jal (50%), Co-director: Boris Vodungbo (50%).

2017 **Ivette Jazmín Bermúdez Macias**, *Development, characterization and first applications of a fs time resolved MOKE setup*, Director: Boris Vodungbo (50%), Co-director: Emmanuelle Jal (50%).

2015 **Xuan Liu**, *Resonant magnetic scattering with soft X-ray pulses to study femtosecond demagnetization of multilayer alloy films*, Director: Boris Vodungbo.

Education

2007 **PhD in materials science**, *Universté Pierre et Marie Curie*, Paris, France.

2004 **Master degree in materials science**, *Université Pierre et Marie Curie*, Paris, France.

2004 **Master degree in physics**, *École Normale Supérieure*, Paris, France.

Funded projects

2022–2025 **HYPNOSE**, *ANR*, 150 k€.

2019–2021 **MADAM**, *Émergence Sorbonne Université*, 60 k€.

2018–2020 **STEROID**, *PICS*, 15 k€.

2018–2020 **2D-Rapide**, *TGI CNRS*, 200 k€.

2017–2018 **XUV10**, *Labex PALM*, 50 k€.

2015–2019 **UMAMI**, *ANR*, 170 k€.

2012–2014 **RAMSES**, *Labex PALM*, 120 k€.

2010–2013 **FEMTO-X-MAG**, *ANR*, 160 k€.

2010 **POL-IMMAGE**, *Triangle de la physique*, 60 k€.

2010 **MagDyn**, *PE/PS SASELELX (CNRS)*, 10 k€.

2009 **IMMAGE**, *Triangle de la physique*, 60 k€.

Publications

1 M. Hennes, G. Lambert, V. Chardonnet, R. Delaunay, G. S. Chiuzbăian, E. Jal and B. Vodungbo. *Element-selective analysis of ultrafast demagnetization in Co/Pt multilayers exhibiting large perpendicular magnetic anisotropy*. *Applied Physics Letters*, **120**, 7, 072408 (2022). doi: 10.1063/5.0080275.

2 X. Liu, E. Jal, R. Delaunay, R. Jarrier, G. S. Chiuzbaian, G. Malinowski, T. Golz, E. Zapolnova, R. Pan, N. Stojanovic, J. Lüning and B. Vodungbo. *Investigating Coherent Magnetization Control with Ultrashort THz Pulses*. *Applied Sciences*, **12**, 3 (2022). ISSN 2076-3417. doi: 10.3390/app12031323.

3 C. Léveillé, K. Desjardins, H. Popescu, B. Vodungbo, M. Hennes, R. Delaunay, E. Jal, D. De

Angelis, M. Pancaldi, E. Pedersoli, F. Capotondi and N. Jaouen. *Single-shot experiments at the soft X-FEL FERMI using a back-side-illuminated scientific CMOS detector*. *Journal of Synchrotron Radiation*, **29**, 1, 103–110 (2022). doi:10.1107/S1600577521012303.

4 K. Légaré, R. Safaei, G. Barrette, L. Arias, P. Lassonde, H. Ibrahim, B. Vodungbo, E. Jal, J. Lüning, N. Jaouen, Z. Tao, A. Baltuška, F. Légaré and G. Fan. *Raman Red-Shift Compressor: A Simple Approach for Scaling the High Harmonic Generation Cut-Off*. *Advanced Photonics Research*, **2**, 11, 2100113 (2021). doi:10.1002/adpr.202100113.

5 X. Liu, A. Merhe, E. Jal, R. Delaunay, R. Jarrier, V. Chardonnet, M. Hennes, S. G. Chiuzbaian, K. Légaré, M. Hennecke, I. Radu, C. V. K. Schmising, S. Grunewald, M. Kuhlmann, J. Lüning and B. Vodungbo. *Sub-15-fs X-ray pump and X-ray probe experiment for the study of ultrafast magnetization dynamics in ferromagnetic alloys*. *Optics Express*, **29**, 20, 32388–32403 (2021). doi:10.1364/OE.430828.

6 V. Chardonnet, M. Hennes, R. Jarrier, R. Delaunay, N. Jaouen, M. Kuhlmann, N. Ekanayake, C. Léveillé, C. von Korff Schmising, D. Schick, K. Yao, X. Liu, G. S. Chiuzbăian, J. Lüning, B. Vodungbo and E. Jal. *Toward ultrafast magnetic depth profiling using time-resolved x-ray resonant magnetic reflectivity*. *Structural Dynamics*, **8**, 3, 034305 (2021). doi:10.1063/4.0000109.

7 M. Hennes, B. Rösner, V. Chardonnet, G. S. Chiuzbaian, R. Delaunay, F. Döring, V. A. Guzenko, M. Hehn, R. Jarrier, A. Kleibert, M. Lebugle, J. Lüning, G. Malinowski, A. Merhe, D. Naumenko, I. P. Nikolov, I. Lopez-Quintas, E. Pedersoli, T. Savchenko, B. Watts, M. Zangrando, C. David, F. Capotondi, B. Vodungbo and E. Jal. *Time-Resolved XUV Absorption Spectroscopy and Magnetic Circular Dichroism at the Ni M2,3-Edges*. *Applied Sciences*, **11**, 1 (2021). ISSN 2076-3417. doi:10.3390/app11010325.

8 M. Hennes, A. Merhe, X. Liu, D. Weder, C. v. K. Schmising, M. Schneider, C. M. Günther, B. Mahieu, G. Malinowski, M. Hehn, D. Lacour, F. Capotondi, E. Pedersoli, I. P. Nikolov, V. Chardonnet, E. Jal, J. Lüning and B. Vodungbo. *Laser-induced ultrafast demagnetization and perpendicular magnetic anisotropy reduction in a* $\mathrm{Co_{88}Tb_{12}}$ *thin film with stripe domains*. *Physical Review B*, **102**, 174437 (2020). doi:10.1103/PhysRevB.102.174437.

9 B. Rösner, B. Vodungbo, V. Chardonnet, F. Döring, V. A. Guzenko, M. Hennes, A. Kleibert, M. Lebugle, J. Lüning, N. Mahne, A. Merhe, D. Naumenko, I. P. Nikolov, I. Lopez-Quintas, E. Pedersoli, P. R. Ribič, T. Savchenko, B. Watts, M. Zangrando, F. Capotondi, C. David and E. Jal. *Simultaneous two-color snapshot view on ultrafast charge and spin dynamics in a Fe-Cu-Ni tri-layer*. *Structural Dynamics*, **7**, 5, 054302 (2020). doi:10.1063/4.0000033.

10 M. Schneider, B. Pfau, C. M. Günther, C. von Korff Schmising, D. Weder, J. Geilhufe, J. Perron, F. Capotondi, E. Pedersoli, M. Manfredda, M. Hennecke, B. Vodungbo, J. Lüning and S. Eisebitt. *Ultrafast Demagnetization Dominates Fluence Dependence of Magnetic Scattering at Co* M *Edges*. *Physical Review Letters*, **125**, 127201 (2020). doi:10.1103/PhysRevLett.125.127201.

11 D. Weder, C. von Korff Schmising, C. M. Günther, M. Schneider, D. Engel, P. Hessing, C. Strüber, M. Weigand, B. Vodungbo, E. Jal, X. Liu, A. Merhe, E. Pedersoli, F. Capotondi, J. Lüning, B. Pfau and S. Eisebitt. *Transient magnetic gratings on the nanometer scale*. *Structural Dynamics*, **7**, 5, 054501 (2020). doi:10.1063/4.0000017.

12 V. Cardin, T. Balciunas, K. Légaré, A. Baltuska, H. Ibrahim, E. Jal, B. Vodungbo, N. Jaouen, C. Varin, J. Lüning et al. *Wavelength scaling of ultrafast demagnetization in Co/Pt multilayers*. *Physical Review B*, **101**, 5, 054430 (2020).

13 C. von Korff Schmising, F. Willems, S. Sharma, K. Yao, M. Borchert, M. Hennecke, D. Schick, I. Radu, C. Strüber, D. W. Engel, V. Shokeen, J. Buck, K. Bagschik, J. Viefhaus, G. Hartmann, B. Manschwetus, S. Grunewald, S. Düsterer, E. Jal, B. Vodungbo, J. Lüning and S. Eisebitt. *Element-Specific Magnetization Dynamics of Complex Magnetic Systems Probed by Ultrafast Magneto-Optical Spectroscopy*. *Applied Sciences*, **10**, 21 (2020). ISSN 2076-3417. doi: 10.3390/app10217580.

14 C. Alves, G. Lambert, V. Malka, M. Hehn, G. Malinowski, M. Hennes, V. Chardonnet, E. Jal, J. Lüning and B. Vodungbo. *Resonant Faraday effect using high-order harmonics for the investigation of ultrafast demagnetization*. *Physical Review B*, **100**, 14, 144421 (2019).

15 E. Jal, M. Makita, B. Rösner, C. David, F. Nolting, J. Raabe, T. Savchenko, A. Kleibert, F. Capotondi, E. Pedersoli, L. Raimondi, M. Manfredda, I. Nikolov, X. Liu, A. e. d. Merhe, N. Jaouen, J. Gorchon, G. Malinowski, M. Hehn, B. Vodungbo and J. Lüning. *Single-shot time-resolved magnetic x-ray absorption at a free-electron laser*. *Physical Review B*, **99**, 144305 (2019). doi:10.1103/PhysRevB.99.144305.

16 B. Mahieu, S. Stremoukhov, D. Gauthier, C. Spezzani, C. Alves, B. Vodungbo, P. Zeitoun, V. Malka, G. De Ninno and G. Lambert. *Control of ellipticity in high-order harmonic generation driven by two linearly polarized fields*. *Physical Review A*, **97**, 043857 (2018). doi:10.1103/PhysRevA.97.043857.

17 M. Buzzi, M. Makita, L. Howald, A. Kleibert, B. Vodungbo, P. Maldonado, J. Raabe, N. Jaouen, H. Redlin, K. Tiedtke et al. *Single-shot Monitoring of Ultrafast Processes via X-ray Streaking at a Free Electron Laser*. *Scientific Report*, **7**, 7253 (2017).

18 D. Weder, C. Von Korff Schmising, F. Willems, C. M. Günther, M. Schneider, B. Pfau, A. Merhe, E. Jal, B. Vodungbo, J. Lüning, B. Mahieu, F. Capotondi, E. Pedersoli and S. Eisebitt. *Multi-Color Imaging of Magnetic Co/Pt Multilayers*. *IEEE Transactions on Magnetics*, , 11, 1–5. ISSN 0018-9464. doi:10.1109/TMAG.2017.2699560.

19 E. Jal, V. López-Flores, N. Pontius, T. Ferté, N. Bergeard, C. Boeglin, B. Vodungbo, J. Lüning and N. Jaouen. *Structural dynamics during laser-induced ultrafast demagnetization*. *Physical Review B*, **95**, 184422 (2017). doi:10.1103/PhysRevB.95.184422.

20 F. Willems, C. v. K. Schmising, D. Weder, C. M. Günther, M. Schneider, B. Pfau, S. Meise, E. Guehrs, J. Geilhufe, A. E. D. Merhe, E. Jal, B. Vodungbo, J. Lüning, B. Mahieu, F. Capotondi, E. Pedersoli, D. Gauthier, M. Manfredda and S. Eisebitt. *Multi-color imaging of magnetic Co/Pt heterostructures*. *Structural Dynamics*, **4**, 1, 014301 (2017). doi:10.1063/1.4976004.

21 C. von Korff Schmising, B. Pfau, M. Schneider, C. M. Günther, D. Weder, F. Willems, J. Geilhufe, E. Malm, L. Müller, B. Vodungbo, F. Capotondi, E. Pedersoli, M. Manfredda, J. Lüning and S. Eisebitt. *Imaging Non-Local Magnetization Dynamics*. *Synchrotron Radiation News*, **29**, 3, 26–31 (2016). doi:10.1080/08940886.2016.1174044.

22 B. Vodungbo, B. Tudu, J. Perron, R. Delaunay, L. Müller, M. H. Berntsen, G. Grübel, G. Malinowski, C. Weier, J. Gautier et al. *Indirect excitation of ultrafast demagnetization*. *Scientific Report*, **6**, 18970 (2016).

23 A. Depresseux, E. Oliva, J. Gautier, F. Tissandier, J. Nejdl, M. Kozlova, MaynardG., G. P., TafziA., LifschitzA., K. T., JacquemotS., MalkaV., T. PhuocK., ThauryC., RousseauP., IaquanielloG., LefrouT., FlaccoA., VodungboB., LambertG., RousseA., ZeitounP. and SebbanS. *Table-top femtosecond soft X-ray laser by collisional ionization gating*. *Nature Photonics*, **9**, 12, 817–821 (2015). ISSN 1749-4885. doi:10.1038/nphoton.2015.225.

24 A. Depresseux, E. Oliva, J. Gautier, F. Tissandier, G. Lambert, B. Vodungbo, J.-P. Goddet, A. Tafzi, J. Nejdl, M. Kozlova, G. Maynard, H. T. Kim, K. T. Phuoc, A. Rousse, P. Zeitoun and S. Sebban. *Demonstration of a Circularly Polarized Plasma-Based Soft-X-Ray Laser*. *Physical Review Letters*, **115**, 083901 (2015). doi:10.1103/PhysRevLett.115.083901.

25 G. Lambert, B. Vodungbo, J. Gautier, B. Mahieu, V. Malka, S. Sebban, P. Zeitoun, J. Luning, J. Perron, A. Andreev, S. Stremoukhov, F. Ardana-Lamas, A. Dax, C. P. Hauri, A. Sardinha and M. Fajardo. *Towards enabling femtosecond helicity-dependent spectroscopy with high-harmonic sources*. *Nature Communications*, **6**, 6167 (2015).

26 Lambert G., Andreev A., Gautier J., Giannessi L., Malka V., Petralia A., Sebban S., Stremoukhov S., Tissandier F., Vodungbo B. and Zeitoun Ph. *Spatial properties of odd and even low order harmonics generated in gas*. *Scientific Report*, **5**, 7786 (2015). doi:10.1038/srep07786.

27 E. Allaria, B. Diviacco, C. Callegari, P. Finetti, B. Mahieu, J. Viefhaus, M. Zangrando, G. De Ninno, G. Lambert, E. Ferrari, J. Buck, M. Ilchen, B. Vodungbo, N. Mahne, C. Svetina, C. Spezzani, S. Di Mitri, G. Penco, M. Trovó, W. M. Fawley, P. R. Rebernik, D. Gauthier, C. Grazioli, M. Coreno, B. Ressel, A. Kivimäki, T. Mazza, L. Glaser, F. Scholz, J. Seltmann, P. Gessler, J. Grünert, A. De Fanis, M. Meyer, A. Knie, S. P. Moeller, L. Raimondi, F. Capotondi, E. Pedersoli, O. Plekan, M. B. Danailov, A. Demidovich, I. Nikolov, A. Abrami, J. Gautier, J. Lüning, P. Zeitoun and L. Giannessi. *Control of the Polarization of a Vacuum-Ultraviolet, High-Gain, Free-Electron Laser*. *Physical Review X*, **4**, 041040 (2014). doi:10.1103/PhysRevX.4.041040.

28 C. von Korff Schmising, B. Pfau, M. Schneider, C. Günther, M. Giovannella, J. Perron, B. Vodungbo, L. Müller, F. Capotondi, E. Pedersoli et al. *Imaging Ultrafast Demagnetization Dynamics after a Spatially Localized Optical Excitation*. *Physical Review Letters*, **112**, 21, 217203 (2014).

29 Moisan N., Malinowski G., Mauchain J., Hehn M., Vodungbo B., Luning J., Mangin S., Fullerton E. E. and Thiaville A. *Investigating the role of superdiffusive currents in laser induced demagnetization of ferromagnets with nanoscale magnetic domains*. *Scientific Report*, **4**, 4658 (2014). doi: 10.1038/srep04658.

30 M. Ducousso, X. Ge, W. Boutu, D. Gauthier, B. Barbrel, F. Wang, A. Borta, A. Gonzalez, M. Billon, B. Vodungbo et al. *Single-shot studies of a Co/Pd thin film's magnetic nano-domain structure using ultrafast x-ray scattering*. *Laser Physics*, **24**, 2, 025301 (2014).

31 X. Ge, M. Ducousso, W. Boutu, B. Tudu, B. Barbrel, D. Gauthier, A. Borta, A.-I. Gonzalez, F. Wang, B. Iwan et al. *Sub-100 nanometer lensless probing of Co/Pd magnetic nanodomains using a table-top femtosecond soft X-ray harmonic source*. *Journal of Modern Optics*, **60**, 17, 1475–1483 (2013).

32 L. Müller, S. Schleitzer, C. Gutt, B. Pfau, S. Schaffert, J. Geilhufe, C. von Korff Schmising, M. Schneider, C. Günther, F. Büttner et al. *Ultrafast Dynamics of Magnetic Domain Structures Probed by Coherent Free-Electron Laser Light*. *Synchrotron Radiation News*, **26**, 6, 27–32 (2013).

33 B. Vodungbo, J. Gautier, G. Lambert, P. Zeitoun and J. Lüning. *Comment on"Ultrafast Demagnetization Measurements Using Extreme Ultraviolet Light: Comparison of Electronic and Magnetic Contributions"*. *Physical Review X*, **3**, 3, 38001 (2013).

34 L. Müller, C. Gutt, B. Pfau, S. Schaffert, J. Geilhufe, F. Büttner, J. Mohanty, S. Flewett, R. Treusch, S. Düsterer et al. *Breakdown of the X-ray resonant magnetic scattering signal during intense pulses of extreme ultraviolet free-electron-laser radiation*. *Physical Review Letters*, **110**, 23, 234801 (2013).

35 W. Ma, B. Vodungbo, K. Nilles, P. Theato and J. Lüning. *Surface and bulk ordering in thin films of a symmetrical diblock copolymer*. *Journal of Polymer Science Part B: Polymer Physics*, **51**, 17, 1282–1287 (2013).

36 W. Ma, B. Vodungbo, K. Nilles, Y. Liu, P. Theato and J. Luning. *Precise structural investigation of symmetric diblock copolymer thin films with resonant soft X-ray reflectivity*. *Soft Matter*, **9**, 37, 8820–8825 (2013).

37 F. Ardana-Lamas, G. Lambert, A. Trisorio, B. Vodungbo, V. Malka, P. Zeitoun and C. Hauri. *Spectral characterization of fully phase-matched high harmonics generated in a hollow waveguide for free-electron laser seeding*. *New Journal of Physics*, **15**, 7, 073040 (2013).

38 B. Pfau, S. Schaffert, L. Müller, C. Gutt, A. Al-Shemmary, F. Büttner, R. Delaunay, S. Düsterer, S. Flewett, R. Frömter, J. Geilhufe, E. Guehrs, C. M. Günther, R. Hawaldar, M. Hille, N. Jaouen, A. Kobs, K. Li, J. Mohanty, H. Redlin, W. F. Schlotter, D. Stickler, R. Treusch, B. Vodungbo, M. Kläui, H. P. Oepen, J. Lüning, G. Grübel and S. Eisebitt. *Ultrafast optical demagnetization manipulates nanoscale spin structure in domain walls*. *Nature Communications*, **3**, 1100 (2012).

39 B. Vodungbo, J. Gautier, G. Lambert, A. B. Sardinha, M. Lozano, S. Sebban, M. Ducousso, W. Boutu, K. Li, B. Tudu, M. Tortarolo, R. Hawaldar, R. Delaunay, V. López-Flores, J. Arabski, C. Boeglin, H. Merdji, P. Zeitoun and J. Lüning. *Laser-induced ultrafast demagnetization in the presence of a nanoscale magnetic domain network*. *Nature Communications*, **3**, 999 (2012).

40 T. Wang, D. Zhu, B. Wu, C. Graves, S. Schaffert, T. Rander, M. Leonard, B. Vodungbo, C. Baumier, D. P. Bernstein, B. Bräuer, V. Cros, S. de Jong, R. Delaunay, A. Fognini, R. Kukreja, S. Lee, V. Lopéz-Flores, J. Mohanty, B. Pfau, H. Popescu, M. Sacchi, A. Barszczak Sardinha, F. Sirotti, P. Zeitoun, M. Messerschmidt, J. J. Turner, W. F. Schlotter, O. Hellwig, R. Mattana, N. Jaouen, F. Fortuna, Y. Acremann, C. Gutt, H. A. Dürr, E. Beaurepaire, C. Boeglin, S. Eisebitt, G. Grübel, J. Lüning, J. Stöhr and A. Scherz. *Femtosecond Single-Shot Imaging of Nanoscale Ferromagnetic Order in CoPd Multilayers Using Resonant X-Ray Holography*. *Physical Review Letters*, **108**, 26, 267403 (2012).

41 B. Vodungbo, A. Barszczak Sardinha, J. Gautier, G. Lambert, M. Lozano, S. Sebban, E. Meltchakov, F. Delmotte, V. Lopez-Flores, J. Arabski, C. Boeglin, E. Beaurepaire, R. Delaunay, J. Lüning and P. Zeitoun. *Table-top resonant magnetic scattering with extreme ultraviolet light from high-order harmonic generation*. *EPL*, **94**, 5, 54003 (2011).

42 B. Vodungbo, A. Barszczak Sardinha, J. Gautier, G. Lambert, C. Valentin, M. Lozano, G. Iaquaniello, F. Delmotte, S. Sebban, J. Lüning and P. Zeitoun. *Polarization control of high order harmonics in the EUV photon energy range*. *Optics Express*, **19**, 5, 4346–4356 (2011). doi:10.1364/OE.19.004346.

43 J. Varalda, C. A. Dartora, A. J. A. de Oliveira, W. A. Ortiz, B. Vodungbo, M. Marangolo, F. Vidal, Y. Zheng, G. G. Cabrera and D. H. Mosca. *Spin-dependent resonant quantum tunneling between magnetic nanoparticles on a macroscopic length scale*. *Physical Review B*, **83**, 045205 (2011). doi:10.1103/PhysRevB.83.045205.

44 P. Schio, F. Vidal, Y. Zheng, J. Milano, E. Fonda, D. Demaille, B. Vodungbo, J. Varalda, A. J. A. de Oliveira and V. H. Etgens. *Magnetic response of cobalt nanowires with diameter below 5 nm*. *Physical Review B*, **82**, 094436 (2010). doi:10.1103/PhysRevB.82.094436.

45 F. Vidal, Y. Zheng, J. Milano, D. Demaille, P. Schio, E. Fonda and B. Vodungbo. *Nanowires formation and the origin of ferromagnetism in a diluted magnetic oxide*. *Applied Physics Letters*, **95**, 15, 152510 (2009). doi:10.1063/1.3250173.

46 B. Vodungbo, F. Vidal, Y. Zheng, M. Marangolo, D. Demaille, V. H. Etgens, J. Varalda, A. J. A. de Oliveira, F. Maccherozzi and G. Panaccione. *Structural, magnetic and spectroscopic study of a diluted magnetic oxide: Co doped $CeO_{2-\delta}$*. *Journal of Physics: Condensed Matter*, **20**, 12, 125222 (2008).

47 Y. Zheng, B. Vodungbo, F. Vidal, M. Selmane and D. Demaille. *Growth and structural analysis of diluted magnetic oxide Co-doped $CeO_{2-\delta}$ films deposited on Si and $SrTiO_3$ (100)*. *Journal of Crystal Growth*, **310**, 14, 3380–3385 (2008). ISSN 0022-0248. doi:10.1016/j.jcrysgro.2008.04.027.

48 V. Garcia, M. Bibes, B. Vodungbo, M. Eddrief, D. Demaille and M. Marangolo. *Magnetic and structural properties of MnAs thin films on GaAs(111)B: Influence of the growth temperature*. *Applied Physics Letters*, **92**, 1, 011905 (2008). doi:10.1063/1.2830012.

49 B. Vodungbo, Y. Zheng, M. Marangolo, D. Demaille and J. Varalda. *Planar assembly of monodisperse metallic cobalt nanoparticles embedded in $TiO_{2-\delta}$ matrix*. *Journal of Physics: Condensed Matter*, **19**, 11, 116205 (2007).

50 J. Varalda, W. A. Ortiz, A. J. A. de Oliveira, B. Vodungbo, Y.-L. Zheng, D. Demaille, M. Marangolo and D. H. Mosca. *Tunnel magnetoresistance and Coulomb blockade in a planar assembly of cobalt nanoclusters embedded in TiO_2*. *Journal of Applied Physics*, **101**, 1, 014318 (2007). doi:10.1063/1.2405728.

51 B. Vodungbo, Y. Zheng, F. Vidal, D. Demaille, V. H. Etgens and D. H. Mosca. *Room temperature ferromagnetism of Co doped $CeO_{2-\delta}$ diluted magnetic oxide: Effect of oxygen and anisotropy*. *Applied Physics Letters*, **90**, 6, 062510 (2007). doi:10.1063/1.2472520.

International Conferences and Workshops

Invited

1 B. Vodungbo. *Probing ultrafast demagnetization with soft X-ray*. International conference on X-ray lasers, Nara, Japan (2016).

2 B. Vodungbo. *Laser-induced ultrafast demagnetization in the presence of a nanoscale magnetic domain network*. Resonant Elastic X-ray Scattering, Oxford, UK (2013).

3 B. Vodungbo. *Application of femtosecond X-rays sources: Laser-induced ultrafast demagnetization in the presence of a nanoscale magnetic domain network*. International conference on X-ray lasers, Paris, France (2012).

Others

1 B. Vodungbo. *Soft X-ray pump – soft X-ray probe experiment with sub-10 fs time resolution for the study of ultrafast demagnetization*. 4th Ultrafast Magnetism Conference 2019, York, UK (2019).

2 B. Vodungbo. *X-ray pump – X-ray probe and X-ray streaking for ultrafast magnetization dynamics*. Journées du GDRi XFEL, Rennes, France (2018).

3 B. Vodungbo. *Role of spin transport in ultrafast demagnetization of Co/Pt and Co/Pd multilayers* . Ultrafast magnetism conference, Nijmegen, Pays-bas (2015).

4 B. Vodungbo. *Probing ultrafast demagnetization with soft X-ray to investigate the role of spin transport in multilayers*. One day conference on Light and Nanomagnetism, Nancy, France (2015).

5 B. Vodungbo. *A soft X-ray view on ultrafast demagnetization*. Workshop on femtomagnetism, Nancy, France (2013).

6 B. Vodungbo. *Ultrafast demagnetization at the nanometer lengthscale*. Workshop on X-Ray View of Ultrafast Dynamics in Solids, BESSY, Berlin, Allemagne (2011).

7 B. Vodungbo, A. Barszczak Sardinha, J. Gautier, G. Lambert, S. Sebban, J. Lüning and P. Zeitoun. *Circularly polarized high order harmonics in the EUV photon energy range: toward table-top nanometric magnetic imaging*. SPIE Conference, X-Ray Lasers and Coherent X-Ray Sources: Development and Applications IX, San Diego, États-Unis (2011). doi:10.1117/12.893603.

8 B. Vodungbo, A. Barszczak Sardinha, J. Gautier, G. Lambert, S. Sebban, P. Zeitoun, K. Li, R. Hawaldar, R. Delaunay and J. Lüning. *Ultrafast demagnetization probed by high order harmonics*. Workshop on magnetization dynamics in the light of pulsed X-ray sources: from storage rings to X-FELs, SOLEIL, Gif-sur-Yvette, France (2011).

9 B. Vodungbo, Y. Zheng, F. Vidal, D. Demaille and V. H. Etgens. *Ferromagnetic properties of Co doped CeO_2*. E-MRS Fall Meeting, Varsovie, Pologne (2006).